

Answers to anonymous referee #1

The authors present new direct measurements of the volatility of biogenic oxidation products, an active area of research in the field, using recently developed inlets for PTR-MS. The major focus of this work are the description of an approach for identifying fragments in PTR-MS data based on measured volatility, demonstration and inter-comparison of 3 sampling systems for PTR-MS, and comparison of measured volatility to theoretical. The conclusions are well supported by the results and the recent literature, and the authors are clearly knowledgeable. The work is robust and valuable, and is in general presented clearly. The authors do a nice job of discussing some of the details and considering all of the possible sources of uncertainty. Though I think there are parts of the discussion and analysis that need to be refined and addressed, as indicated below, none are too scientifically substantial -only minor revisions are necessary for publication.

Answer: We do appreciate the positive assessment. We have addressed the various comments and suggestion of the referee as described below. Changes in the manuscript are highlighted in *italic*.

That said, my major concern is that I'm not completely convinced this publication is the proper journal, and wonder whether a more appropriate venue would be Atmospheric Measurement Techniques. Though some of the final conclusions and summary do get at scientific implications of the work, a substantial focus of the manuscript as currently written is devoted to developing an approach for identifying fragments in an instrument (Fig. 1), comparing between sampling approaches (Fig. 2), and demonstrating the capabilities of the approach (Fig. 3). Consequently, it reads somewhat more like it focuses on the techniques than the implications or results. I think it could go a bit either way, and leave it up to the editor, but would argue that it should perhaps go to AMT instead of ACP.

Answer: We understand the dilemma of the referee given that our study includes both elements of method development and also its application and scientific outcome in chamber studies. However, Fig.3, Fig. 4 and Fig. 5, do show results of direct volatility measurements of major biogenic oxidation products and their comparison to theoretical approaches. To our knowledge these scientific findings represent new valuable insights that extend beyond just the comparison of different atmospheric measurement techniques. We do agree that an essential step in order to achieve a reliable conclusion for this study was the development of a method to exclude possible fragments. Nonetheless, this method has only been used as a tool in order to narrow down the uncertainties and provide more reliable conclusions for the above figures.

Major comments:

Throughout the discussion and presentation of this work, the authors seem to go back and forth somewhat on the lines between ions and molecules. At some points, the fact that the PTR-MS measures ions without structure is a major focus of the discussion. At others, figures and text seem to imply that this work is measuring one specific molecule. Often the authors later clarify, but it makes the discussion somewhat "blurry." As an example, the inset of Figure 4 strongly implies they are measuring nopinone, the fact that it is actually an ion with suggested by unknown structure is not discussed until 40 lines later and not mentioned in the figure. I recommend the authors state clearly when they are discussing ions they measured, vs. when they are discussing specific molecules, and generally shore up their language around these issues. It is a major point in comparing measured vs. theoretical volatility, which they acknowledge, but only really discuss near

the end of the manuscript. I think a little reorganization would probably address the issue. This also confuses the assumptions around fragmentation, since without structure their assumptions that loss of an e.g. C and O atom will increase volatility are not necessarily true (see below). I think their case could still be made, but it needs to be made a bit more carefully, and the fact that PTR measures ions, not structures is part of that discussion.

Answer: Changes in order to further clarify when the discussion is focused on ions and when the assumption of a chemical structure is implied were performed throughout the text as following:

- For Figure 4 the phrase “*suggested structure*” was added on top of the compounds.
- Line 427: Replaced “compounds” with “ions”.
- Line 454: Changed “Species detected as parent ions that overlapped with compounds from previous publications were further examined based on their structural information” to “*By attributing a chemical structure to the ions identified by the PTR-MS, detected parent ions that overlapped with compounds from previous publications were further examined based on their structural information*”
- Line 456: Added “*Uncertainties introduced by assigning a chemical structure to an ion of a given chemical formula are further discussed in this section.*”

Comparisons between the ACM, TD, and CHARON are a major part of this work, but there is no real description of them. I recognize that the authors cite their previous work(s) for descriptions, but given the role of these comparisons in this work, at least some cursory description should be provided. How do they differ (other than temperatures and pressures)?

Answer: We added a paragraph giving the important difference in the set-up of each instrument to highlight the similarities and difference of the instruments. The changes in the manuscript are as follows:

“In the following, the most important characteristics and parameters are described briefly. The CHARON inlet combines a gas phase denuder, an aerodynamic lens with an inertial sampler and a thermal desorption unit which is coupled to a PTR-ToF-MS. The gas phase denuder removes gas phase analytes. Subsequently the aerosols are collimated by the aerodynamic lens and a particle enriched sample flow is achieved by the inertial sampler. Afterwards the particles pass through a thermal desorption unit in which the particles are volatilized before transferred to the gas phase detector. The ACM has two sample air inlets. For the gas phase inlet air passes through a PTFE particle filter and is then directly introduced into the PTR-MS. For particle collection via the second sampling line air is passing through an aerodynamic lens removing gas phase and collimating particles onto a beam. The particles are subsequently passing a vacuum chamber and are collected on a cooled sampling surface. Once collection is finished particles are desorbed and transferred via a carrier gas (N₂) to the PTR-ToF-MS detector. Important to note is that during the collection process the PTR-ToF-MS is measuring the gas phase in parallel allowing for quasi simultaneous characterization of gas and particle phase. The TD also employs a gas phase denuder to remove gas phase analytes before the aerosols are impacted using a Collection and Thermo-Desorption (CTD) cell. After collection particles are thermally desorbed and the components transferred to the PTR-ToF-MS. In the following, operational parameters are listed for all PTR-based instruments. The CHARON is a real time measurement (10 s integration time in the detector), while the ACM and TD have sampling times for this study of 120 min and 240 min, respectively.”

and

“The operational conditions for each PTR-ToF-MS were different with regard to a different electric field strength ($V\text{ cm}^{-1}$) to buffer gas density (molecules cm^{-3}) ratio (E/N). This can lead to different ionic fragmentation behavior. Therefore, the overlap of parent ions measured between the different instruments can be reduced. A detailed discussion about the E/N effect has been investigated by Gkatzelis et al. (2018a). Operational details for the different PTR-ToF-MS conditions are given also in Table S2.”

The authors often paint thermal and ionic fragmentation with one brush. In some ways that makes sense, I understand, but I don't think I fully agree they should be lumped. Thermal fragmentation is measurement of a molecule that was actually present in the particle as part of an accretion product. Ionic fragmentation is measurement of a molecule that was never in the ambient sample. In some cases this is a meaningful distinction. One major example is the decision to call VOCs fragments and exclude them from future analysis, yet IVOCs are included, even though they are almost certainly thermal fragments in many cases. Essentially the authors have decided that VOCs ($C < 6$, $O < 1$) are too small to be in the particle so are referred to as fragments, yet nopinone is included in the discussion, and later said to possibly come from thermal fragmentation. So then, what is the distinction between nopinone, which the authors continue to include, and those ions deemed "fragments" and excluded? Shouldn't VOCs thus be included in all the later analyses, and in the mass pie charts? They were, after all, observed in the particle phase. Or should those IVOCs be colored as fragments in Figure 1? Also, the described approach to identifying fragments makes sense for ionic fragments, but not for thermal fragments, which may or may not have the same volatility as their parent (which may or may not be measured). Similarly, ionic fragmentation will likely have a relatively small impact on volatility, while thermal fragmentation probably has a substantial one. So this approach captures one pathway but not the other, suggesting discussion would be clearer if these two processes were more distinctly discussed. Overall, I think thermal and ionic fragmentation should not be treated together, for instance in Figure 1 and in discussion there and elsewhere (e.g. Section 3.1, lines 496, 593). They have different causes and different implications.

Answer: Thermal fragmentation can indeed be a result of already existing molecules that were present in the particle as part of an accretion product but this is not proven to be the only possible fragmentation pathway. Exposure of molecules during desorption to high temperatures for long residence times may initiate the breakage of carbon-carbon or carbon-oxygen bonds thus resulting to a variety of possible fragmentation pathways including the generation of fragment molecules that were not in the ambient sample before. Furthermore, although ionic fragmentation is dominated by the suggested loss pathways included in the method, examples of stronger loss processes do exist. A characteristic example is the detection of monoterpenes. Although PTR-MS detects monoterpenes at m/z 137.13 as $C_{10}H_{16}H^+$, a high signal is also found in m/z 81.07 as $C_6H_9^+$. This difference will result in a relatively large impact on volatility that is directly linked to ionic and not thermal fragmentation. Therefore, a clear separation of thermal and ionic dissociation in these complex systems can be challenging. Nevertheless, although the current state of knowledge does not support a clear separation of thermal and ionic fragmentation, our method is capable of excluding all detectable fragments, independent of their origin. Currently, a detailed lab characterization of the different techniques, at different operating conditions is performed to further address differences and possible thermal and ionic fragmentation pathways.

We do agree with the reviewer that the limits chosen for this method ($C < 6$ and $O < 1$) might be uncertain but based on various publications, that we make the reader aware of in the manuscript, it is indubitable that compounds below this carbon and oxygen atom number, considered VOCs, will be

in the gas-phase. On the contrary, various studies have been performed (Kahnt, 2012; Hohaus et al., 2015) where focus was given on the partitioning of compounds in the IVOC range. These compounds and for example nopinone have troubled the scientific community the last years regarding to why experimental results repeatedly show more in the particle-phase than predicted from theory. A major scientific question and the focus of many recent studies (Shiraiwa et al., 2011) has been towards understanding the phase-state of the particles which could strongly affect the partitioning of compounds in the IVOC and SVOC range. Results from this work further address these questions and limit the possible explanations to either thermal fragmentation or particle phase-state. Excluding completely IVOCs from this method as fragments would imply that we are certain that the phase-state of the particles does not affect the partitioning of these compounds and that thermal fragmentation is the key process, something which is not yet known and could thus bias the results of this study.

Minor comments:

There are significant grammatical errors and language quirks that belie the author as not a non-native English speaker. I have flagged many, but probably not all, below.

Answer: We have corrected all errors mentioned and improved the language of the manuscript where necessary.

The introduction generally covers the topics, but it seems like often references are a bit out of place, missing, or not quite correct. I have tried to note these cases below.

Answer: The introduction was improved according to the suggestions.

Technical comments:

line 47-48: "a detailed understanding...needs to be well defined" is odd English. Re-word.

Answer: The sentence was changed in the manuscript to:

A detailed understanding of SOA formation and composition is critical to develop strategies needs to be well defined for impact mitigation.

line 54: missing comma between "pressures" and "thus"

Answer: Added

line 76: "when applicable" can be deleted. Also, some of the cited works are indeed measuring ions, but others are measuring identified compounds, which is a potentially significant distinction as different molecules of the same formula may partition differently (as discussed latter). See Thompson et al. *Aerosol Sci. Tech.*, 2016, doi: 10.1080/02786826.2016.1254719. Also, citations should probably include Zhao et al., *ES&T*, 2013, doi: 10.1021/es304587x

Answer: We added the following two sentences to the manuscript:

Simultaneous measurements of the gas- and particle-phase mass of organic molecules has also been recently developed using the TAG system sampling alternately with and without a gas phase denuder

in front of the inlet (Zhao et al., 2013) and the modified semi-volatile TAG (SV-TAG) that utilizes two TAG cells in parallel (Isaacman-VanWertz et al., 2016).

and

Measurements of instruments providing molecular identification (e.g. SV-TAG) and measurements from instruments providing identification of ions (e.g. different Chemical Ionization Mass Spectrometer (CIMS)) can be combined to increase the understanding of partitioning of some compounds classes. This was shown in an field intercomparison investigating gas-particle partitioning of oxygenated VOCs during the Southern Oxidant and Aerosol Study (SOAS) (Thompson et al., 2016).

line 79: For 2D-TAG, a more appropriate citation is probably Goldstein et al. J. Chrom. A, 2008, doi:10.1016/j.chroma.2007.09.094. I note that most TAG applications are not 2D, so it should be specific in the name here.

Answer: Corrected

line 85: For SV-TAG, citation should include Zhao et al., Aerosol Sci. Tech., 2013, doi: 10.1080/02786826.2012.747673

Answer: Added

line 86: I don't disagree with the 10-40% estimate, but it should be cited.

Answer: Added

line 95: Krechmer is one of many approaches to estimating c^* , and in fact is one of the more complex ones. I might also recommend citing Daumit et al., Faraday Disc., doi: 10.1039/c3fd00045a and Li et al., ACP, 2016, doi:10.5194/acp-16-3327-2016. Those two references directly parameterize by formula, which seems to be the reference in this sentence.

Answer: Added

line 113: "Deviations...to" is a bit odd. Maybe "deviations between the theoretical and experimental"

Answer: Done

line 130: should be "allows experiments to be conducted"

Answer: Done

line 149: should be "extent"

Answer: Done

line 168: Is it not a problem that the ACM is at sub-freezing temperatures? Does this not result in some gas-phase adsorption? I'm not sure because the description is sparse. Though the instruments are described elsewhere, given that this manuscript focuses in part on intercomparison, it would be helpful to include a few lines of description about each technique.

Answer: The ACM inlet is constructed similar to an Aerodyne Aerosol Mass Spectrometer meaning the sampling air passes through an aerodynamic lens and subsequently through a high vacuum chamber before the particles are impacted on a sub-zero cooled collection surface. So the gas phase

is efficiently removed before particle sampling. We added a more detailed description to the instrument to highlight that fact. Please see answer above.

line 178: Why was the PTR operating differently for each collector? Could this have any impact, or is it calibrated for?

Answer: The PTR-ToF-MS detector of each instrument was operated during the measurement campaign using best practice by each of the respective groups to achieve optimal measurement results. In a nutshell the PTR-ToF-MS E/N settings have to be set to optimize the conditions balancing sensitivity versus ionic fragmentation. As discussed in detail in Gkatzelis et al. 2018 differences in the measurement results obtained from the different instrument originates predominantly from the detector settings and not from the differences in the aerosol sampling inlets which was unexpected. Therefore, in future studies it is advised to try to reduce the difference in PTR detector operations between the different instruments. However, the major impact for the instruments which were operating at higher E/N settings is that we fragment more molecules during ionization compared to lower E/N settings. That means that we limited our analysis since we excluded any ion signal which originates from ionic fragmentation. It is likely that with the same E/N settings in each instrument we would be able to identify more parent ions showing minor ionic fragmentation. Therefore, it has no impact on the identified parent ions and the main conclusion only on the amount of identified parent ions and the overlap of identified parent ions between instruments.

line 187: Do I correctly understand that all gas-phase measurements are thus passed through a filter? If so, I think this could substantially bias the measurements toward removal of gas-phase compounds and so higher measured particle partitioning. How was this checked or corrected for?

Answer: Only the PTR-MS of the ACM was operated by passing the gas-phase measurements through a filter. To make this clear the sentence was changed to “... was additionally introduced to the PTR-MS line of the ACM to reassure complete particle-phase removal.”

Detailed discussion concerning the differences related to the gas-phase measurements of the two PTR-MS are in lines 430 to 447.

line 204: "pptV" here and elsewhere doesn't need to be capitalized

Answer: Changed in line 204, 207, and Table 1

line 206: should read "additional"

Answer: Done

line 220: if I'm not mistaken, this equation should use the molecular weight of the absorbing material, not the compound being absorbed. It looks like that is what is done, but is not what is stated in the description.

Answer: We thank the reviewer for noticing this error.

line 253: relationship between temperature of c^* is log-linear, so a deviation of 15 degrees should vary c^* by a multiplier, not a specific number (e.g. 10 times, not 10 $\mu\text{g}/\text{m}^3$)

Answer: The sentence was changed to “...with changes of $\pm 15^\circ\text{C}$ resulting in a C^* change by a factor of 10.”

line 253: I'm not completely convinced those temperature variations are as negligible as the authors seem to assume. Take for example the mixture experiment, with SOA concentrations of 60 $\mu\text{g}/\text{m}^3$. A

compound with a c^* of 60 $\mu\text{g}/\text{m}^3$ at 25 degrees (e.g a triol with 7 or 8 carbons, based on SIMPOL) has a c^* of 10 $\mu\text{g}/\text{m}^3$ at 15 degrees, the range of temperatures in the experiment. That is the difference of 0.8 log units, and means that in the experiment it is the difference between half in the particle and 85% in the particle. Not a huge difference, perhaps, but enough to potentially be a source of uncertainty given the error bars on Figure 1, and probably worth exploring and discussing.

Answer: We agree that the assumption can be improved and therefore, uncertainties were further examined with a focus on the β -pinene oxidation products. An overview of the temperature dependence was calculated from the theoretical approaches and added as a figure in the supplementary material (Figure S7). Figure S7 was also added at the end to these answers below. These uncertainties were dependent on the structure of the compounds and ranged from 0.3 to 0.6 in $\log(C^*)$. These uncertainties are discussed in the text as follows:

"The uncertainty added from these variations (< 10 °C) was further examined with a focus on the β -pinene oxidation products (Figure S7). Difference in volatility due to variations ranged from 0.3 to 0.6 $\log(C^)$ units depending on the chemical structure of the compound. Nevertheless, these variations can be considered small and not strongly affecting the conclusions of this work."*

line 294-295: it is a bit confusing to say their volatility ranged from 1 to 4. Maybe just say " 10^1 to 10^4 $\mu\text{g}/\text{m}^3$ "

Answer: Done

lines 298-304: I agree that ions that small are likely fragments, but this does not mean that larger ions are not, so the cutoff to include above and disregard below feels a bit arbitrary. See general comments above.

Answer: Please refer to the answer to the third major comment.

lines 307-309: This assumption of functional groups decreasing volatility makes sense for pure components, but disregards potential impacts of structure. For example if the ion $\text{C}_8\text{H}_{12}\text{O}_2$ represents a dione, the ion $\text{C}_7\text{H}_{12}\text{O}$ could be an alcohol so be held in a polar particle by stronger hydrogen bonding. I'm not totally convinced that without knowing structures the authors can denitively claim that 2 ions that differ by the atoms that could be a functional group will necessarily have a given relationship in volatility. Previous work (e.g. the Isaacman-VanWertz et al., 2017 reference cited in the manuscript) has used correlation of the timeseries of ions to assess potential overlap, could something similar not be included in this analysis to confirm that fragments covary in time as well as volatility? Also, how did the authors deal with nitrates, given that some of the ions contain nitrogen, is loss of the nitrate group possible and/or considered?

PTR-ToF-MS provides information regarding the chemical formula of a compound and not the chemical structure as would for example a GC-MS. As correctly mentioned, this can lead to the identification of a parent ion as a fragment although it may not be. Nevertheless, although this method will potentially exclude compounds that are parent ions, it will still discard any possible fragments. Correlation analysis based on the time series of the different compounds is a very good way to further improve this method but unfortunately for this work not feasible due to the low time resolution. These points are further discussed in the manuscript as follows:

"It should be noted that PTR-MS provides information regarding the chemical formula of an ion and thus disregards potential impact of the chemical structure. Functionality effect (e.g. stronger hydrogen bonding of an alcohol in a polar particle) can lead to a misidentification of potential parent ions as a fragment using the above described method due to the fact that a lower volatility is

determined compared to an expected volatility based on the chemical formula. Nevertheless, although this method will potentially exclude parent ions, it will still discard also any possible fragments. Correlation analysis based on the time series of the different compounds could further improve the parent ion identification. However due to the low time resolution in this work a time series analysis is not applicable. Another implication relies on the fact that $[M+H]^+$ ions could result from the decomposition of accretion reaction products or oligomers, consequently leading to an overestimation of their particulate phase concentrations."

Organic Nitrates strongly fragment in the PTR-MS and almost certainly lose their nitrate group during ionization with H_3O^+ (Marius Duncianu et al., 2017). Since no compound was identified as an organic nitrate for the limonene experiment, this fragmentation pathway was not chosen in this method since there was no larger molecule to compare to. This is now further mentioned in the manuscript as follows:

"Checks were also performed for loss of the (-HNO₃) functional group for the limonene-NO₃ oxidation experiment but due to the high E/N operating conditions of all PTR-ToF-MS systems, no organic nitrates were identified."

line 333: "promoted" should be "supported"

Answer: Done

line 359: "0.5 volatility resolution" sounds odd. Maybe add "bin" or units

Answer: Added "bin"

line 381: missing "and"

Answer: Added.

line 406: the authors are referring here to the oxidation state of the carbon within the compounds, so should use OS_C as the abbreviation

Answer: Done.

line 442: For tree emissions in Fig. S5, it looks to me like there is significant bias between the two approaches, not just random noise. Why might that be true for only this experiment? Does this imply anything for the other comparisons?

Answer: The reason of this difference is due to the higher complexity of the tree emissions in comparison to the single precursor oxidation experiments. As has been shown from Gkatzelis et al. (2018b), the tree emissions experiment was the only experiment where ions with up to 20 carbon atoms were identified from CHARON when operated at low E/N conditions. These ions fragmented differently in the PTR-MS when operated at different conditions and thus introduced a larger deviation from the one to one line as shown in Fig. S5. Additional information to make this point clear was added in the manuscript:

"Moreover, the tree emissions experiment showed the highest complexity in comparison to the single precursor oxidation experiments, with detected ions that had up to 20 carbon atoms in the particles. These higher molecular weight ions fragmented differently when passing through the differing ToF interfaces and thus resulted to the observed higher deviation."

line 444: remove "existed"

Answer: Corrected.

line 461: misspelled "yielded"

Answer: Corrected.

lines 461-477: The detailed discussion of differences between vapor pressure estimation techniques do not seem necessary here. While it is a nice overview, it feels fairly tangential to the focus of the paper and could be removed or moved to the SI.

Answer: These sentences are moved to the SI and a sentence is added saying: *"More details regarding the theoretical calculations are provided in the Supplement."*

lines 478-479: In the initial discussion of Figure 4, and in Figure 4 itself, the authors seem to imply they are measuring e.g. "nopinone" not just an ion of the same formula. They go on to have a good discussion of this fact, but it should be made clear throughout the discussion and in the figure. (In other words, the inset of Figure 4 is not really an apples-to-apples comparison, which should be clear).

Answer: Please see answer to the first major comment above.

line 504: This approach to constraining the uncertainty due to structure is nice, but its description is a little unclear. "within the estimated uncertainty" of what -the experimental values, or the theoretical nopinone values?

Answer: The sentence was changed to:

"For the β -pinene experiment the isomers showed theoretical C^ values within the estimated uncertainty thus biasing to a minor extent this comparison."*

line 529: misspelled "AIOMFAC"

Answer: Corrected.

line 534: particle phase is humidity dependent, these experiments are at 55%, which could sort of go either way, liquid or solid, for instance see Bateman et al., Nature Geo, 2015, DOI: 10.1038/NGEO2599

Answer: The discussion of the aerosol phase state was put into context to the experimental conditions in this study. The manuscript was revised as follows:

The experimental conditions in this study (on average 55 % RH) suggest that a significant portion of the SOA can be in a semi-solid or glassy state (Bateman et al., 2015).

Figure 2: Re-label as a-h, not 1a-2d.

Answer: Corrected.

Figure 3: I found sizing by oxygen number to be quite confusing. I recognize the utility of it in Figure 1, but in this figure that information is already more or less captured by the axes, and it serves to highlight certain ions for no real scientific reason. Sizing by concentration or not at all might be more appropriate here.

Answer: We removed the sizing by oxygen for Figure 3 and also for Figure S4 to be consistent.

Figure 5: On some monitors, the dashed lines to isomers cannot be seen. Perhaps darken or color them.

Answer: Corrected.

References

Gkatzelis, G. I., Tillmann, R., Hohaus, T., Müller, M., Eichler, P., Xu, K. M., Schlag, P., Schmitt, S. H., Wegener, R., Kaminski, M., Holzinger, R., Wisthaler, A., and Kiendler-Scharr, A.: Comparison of three aerosol chemical characterization techniques utilizing ptr-tof-ms: A study on freshly formed and aged biogenic soa, *Atmos. Meas. Tech.*, 11, 1481-1500, 10.5194/amt-11-1481-2018, 2018a.

Gkatzelis, G. I., Tillmann, R., Hohaus, T., Müller, M., Eichler, P., Xu, K. M., Schlag, P., Schmitt, S. H., Wegener, R., Kaminski, M., Holzinger, R., Wisthaler, A., and Kiendler-Scharr, A.: Comparison of three aerosol chemical characterization techniques utilizing ptr-tof-ms: A study on freshly formed and aged biogenic soa, *Atmos Meas Tech*, 11, 1481-1500, 10.5194/amt-11-1481-2018, 2018b.

Hohaus, T., Gensch, I., Kimmel, J. R., Worsnop, D. R., and Kiendler-Scharr, A.: Experimental determination of the partitioning coefficient of β -pinene oxidation products in soas, *Phys Chem Chem Phys*, 17, 14796-14804, 10.1039/C5CP01608H, 2015.

Kahnt, A.: Semivolatile compounds from atmospheric monoterpene oxidation PhD, Fakultät für Chemie und Mineralogie, Universität Leipzig, Leipzig, Germany, 205 pp., 2012.

Shiraiwa, M., Ammann, M., Koop, T., and Pöschl, U.: Gas uptake and chemical aging of semisolid organic aerosol particles, *P Natl Acad Sci USA*, 108, 11003-11008, 10.1073/pnas.1103045108, 2011.

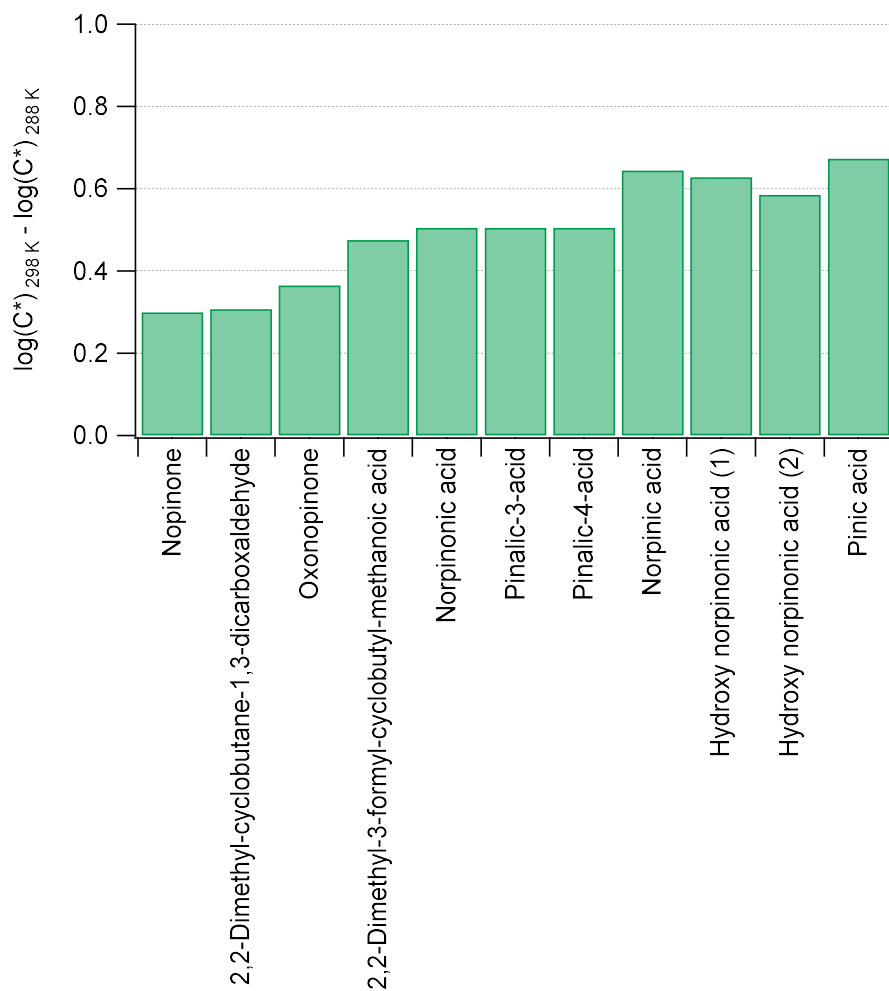


Figure S7: Theoretical calculation of the vapor pressure (y-axis) using the combination of 7 different approaches. To estimate the uncertainty in the experiments due to changes in temperature calculations were also performed at 295 K. Difference in vapor pressure are between 0.3 to 0.6 $\log(C^*)$.

Answers to anonymous referee #2

Gkatzelis and coworkers report measurements of gas-to-particle partitioning of products from biogenic oxidation using three recently developed aerosol inlets and parallel gas-phase measurement. They developed an approach for identifying fragments in data due to thermal dissociation and ionic dissociation. The authors did a decent job in discussing C* intercomparison of 3 aerosol sampling systems and comparison of measured volatility to theoretical calculations. This PTR-based technique can be implemented to promote research in this area. The paper is generally well written. It has a heavy focus on techniques and how they affect the results. I understand that more details are in the cited Gkatzelis (2017) and some are discussed later in the Results section. However, I feel the authors should provide a little more information when relevant and/or refer to the specific section that you discussed in more detail (see specific comments).

We thank the Reviewer for all the comments. We increased the clarity by adding information regarding the measurement techniques and how the differences between the instruments might and can influence the results. For details please see our answers below and also answers to Reviewer 1.

Specific comments:

Line 82: Should be “known”.

Answer: Corrected.

Line 86: Where does the 10-40% come from? Please cite relevant references.

Answer: Please see answer to a similar comment of Reviewer 1.

Line 173: Why ACM and TD have different final temperature? How does this affect the compounds they measured?

Answer: Each instrument was operated during the measurement campaign using best practice by each of the respective groups to achieve optimal measurement results based on previous experience. One expected effect is that the ACM might not desorb and detect compounds which are in the additional temperature range covered by the TD. Therefore, the ACM might measure less compounds than the TD but this would have no influence on the results since we restrict the analysis to measured ions which we identify with our method as likely being parent ions.

Line 176-183: The PTRs were operated under different conditions. When you calculate C* using G/P ratio measured by different PTRs (e.g., TD for particle, a standalone PTR for gas), how did you treat the different sensitivities? In addition, a very simple schematic in SI, or table, showing all the instruments connected to the chamber might be helpful to readers, since the authors refer to the different operating conditions, inlets etc. frequently in discussion. Some time series examples of each technique in SI, along with Figure S1, will also be useful.

We included in the SI Table S2 which shows the details of the conditions for every PTR-ToF-MS used in this study. Difference in sensitivities of the two instruments did not affect this comparison but the main source of uncertainty was introduced due to the different E/N operating conditions. This is now discussed in more detail in the manuscript and has been the main focus of our previous publication (Gkatzelis et al., 2018). The following sentence is added in the manuscript and also the suggested

example time series in the SI in Figure S8. Figure S8 was also added at the end to these answers below.

“Finally, differences in sensitivity for each PTR-MS introduced minor deviations in this study and are discussed in detail in Gkatzelis et al., (2018). A characteristic timeseries of a major oxidation product from the β -pinene ozonolysis for the three different techniques can be found in Figure S8.”

Line 187: It sounds like the PTFE filter is always before the ACM-PTR-MS then how can the ACM collect particles?

Answer: The description of all instruments was significantly extended in the instrumental section of the manuscript. For all details please see answer to Reviewer 1. The fact that the ACM measures both, gas- and particle phase, was especially clarified. The relevant changes in the manuscript are as follows:

“The ACM has two sample air inlets. For the gas phase inlet air passes through a PTFE particle filter and is then directly introduced into the PTR-MS. For particle collection via the second sampling line air is passing through an aerodynamic lens removing gas phase and collimating particles onto a beam. The particles are subsequently passing a vacuum chamber and are collected on a cooled sampling surface. Once collection is finished particles are desorbed and transferred via a carrier gas (N₂) to the PTR-ToF-MS detector. Important to note is that during the collection process the PTR-ToF-MS is measuring the gas phase in parallel allowing for quasi simultaneous characterization of gas and particle phase.”

Line 252: Please be explicit what typical vaporization enthalpies are.

Answer: Added.

Line 253: A change of 15 C will result in C* change larger than 10 ug/m³. For example, a compound with a C*=100 ug/m³ at 290 K will have a C*=700 ug/m³ at 303 K. It is worth to consider and discuss this in the following comparison.

Answer: Please see the answer to Reviewer 1 for the same question.

Line 286: Can the authors estimate the uncertainty caused by operating gas and particle phase measurements under different ionic dissociation?

Answer: Ionic dissociation in the PTR-MS detector is compound dependent. Therefore, a general uncertainty cannot be estimated/applied to the different E/N conditions of the PTR detector. Due to the thermal desorption of the particle phase thermal fragmentation occurs additional to the ionic fragmentation for the particle composition measurements. Since it is not possible to distinguish thermal fragmentation from ionic fragmentation with our measurement techniques estimating uncertainties is not feasible.

Line 317: Did the authors do similar test for organic nitrate products (-HNO₃)?

Answer: Please see the answer to comment of previous reviewer regarding lines 307-309 in the manuscript.

Line 342: Should be “percentage”.

Answer: Corrected.

Line 354: Should be “previous”.

Answer: Corrected.

Figure 2: The error bar for the green dots need a darker color since it's hard to see. The ACM C*s don't have any error bar. Why, too small? In addition, since only averages were presented, it'd be worth to mention in section 2.4 that you calculated C* from equation 2 using how many samples for each technique for each experiment. As temperature varied though an experiment, how was C* affected?

Answer: Colors were changed for Figure 2. ACM had the lowest time resolution thus the number of data points was the lowest in comparison to the other instruments. This is the main reason why the error bars are lower for ACM in comparison to TD and CHARON. In Section 2.4 additional sentences were added:

“Calculation of the average C for every experiment was performed based on the time resolution of each instrument (section 2.2). When the signal in the particle-phase was close to the detection limit and introduced a high uncertainty, the calculation of the C* was not performed.”*

Figure S6: Temp = 280K, why inconsistent with 298K used for experimental measurement mentioned at line 256? The name for each theoretical calculation is not consistent with that in the text, e.g., nano vs. NN.

Answer: The Figure S7 (see also answer to Reviewer 1) was added in order to be consistent with the temperature and the text. Also, this Figure was used in comparison to S6 to determine additional uncertainties in the theoretical calculations use during the subsequent analysis. For further details please see also answers to Reviewer 1 about uncertainty in theoretical vapor pressure calculation.

References

Gkatzelis, G. I., Tillmann, R., Hohaus, T., Müller, M., Eichler, P., Xu, K. M., Schlag, P., Schmitt, S. H., Wegener, R., Kaminski, M., Holzinger, R., Wisthaler, A., and Kiendler-Scharr, A.: Comparison of three aerosol chemical characterization techniques utilizing ptr-tof-ms: A study on freshly formed and aged biogenic soa, *Atmos Meas Tech*, 11, 1481-1500, 10.5194/amt-11-1481-2018, 2018.

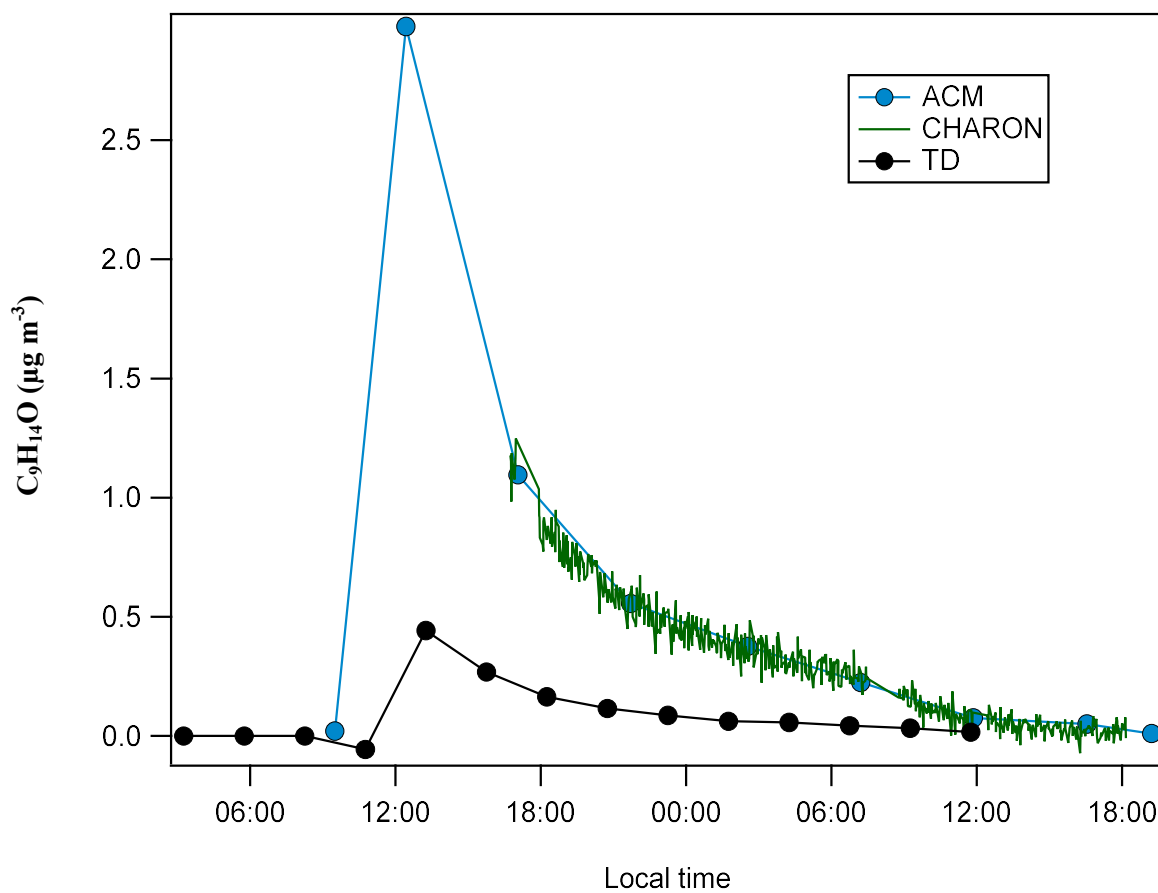


Figure S8: Characteristic example of the timeseries of $C_9H_{14}O$ for the three different inlet techniques

1 Gas-to-particle partitioning of major biogenic oxidation products: A 2 study on freshly formed and aged biogenic SOA

3 Georgios I. Gkatzelis¹, Thorsten Hohaus¹, Ralf Tillmann¹, Iulia Gensch¹, Markus Müller^{2,4},
4 Philip Eichler^{2†}, Kang-Ming Xu³, Patrick Schlag^{1††}, Sebastian H. Schmitt¹, Zhujun Yu¹,
5 Robert Wegener¹, Martin Kaminski¹, Rupert Holzinger³, Armin Wisthaler^{2,5}, Astrid Kiendler-Scharr¹

6
7 ¹ Institute of Energy and Climate Research, IEK-8: Troposphere, Forschungszentrum Jülich GmbH, Jülich, Germany

8 ² Institut für Ionenphysik und Angewandte Physik, Universität Innsbruck, Innsbruck, Austria

9 ³ Institute for Marine and Atmospheric research Utrecht, Princetonplein 5, 3584 CC, Utrecht, The Netherlands

10 ⁴ Ionicon Analytik GmbH, Innsbruck, Austria

11 ⁵ Department of Chemistry, University of Oslo, Norway

12
13 † Now at: German Environment Agency, Dessau-Roßlau, Germany

14 †† Now at: Institute of Physics, University of Sao Paulo, Sao Paulo, Brazil

15

16 Correspondence to: T. Hohaus (t.hohaus@fz-juelich.de)

17 Abstract.

18 Secondary organic aerosols (SOA) play a key role in climate change and air quality. Determining the fundamental
19 parameters that distribute organic compounds between the phases is essential, as atmospheric lifetime and impacts change
20 drastically between gas- and particle-phase. In this work, gas-to-particle partitioning of major biogenic oxidation products
21 was investigated using three different aerosol chemical characterization techniques. The aerosol collection module (ACM),
22 the collection thermal desorption unit (TD) and the chemical analysis of aerosol on-line (CHARON) are different aerosol
23 sampling inlets connected to a Proton Transfer Reaction-Time-of-Flight-Mass Spectrometer (PTR-ToF-MS). These
24 techniques were deployed at the atmosphere simulation chamber SAPHIR to perform experiments on the SOA formation and
25 aging from different monoterpenes (β -pinene, limonene) and real plant emissions (*Pinus sylvestris* L.). The saturation mass
26 concentration C^* and thus the volatility of the individual ions was determined based on the simultaneous measurement of
27 their signal in the gas- and particle-phase.

28 A method to identify and exclude ions affected by thermal dissociation during desorption and ionic dissociation in the
29 ionization chamber of the PTR-MS was developed and tested for each technique. Narrow volatility distributions with organic
30 compounds in the semi-volatile (SVOCs) to intermediate volatility (IVOCs) regime were found for all systems studied.
31 Despite significant differences in the aerosol collection and desorption methods of the PTR based techniques, comparison of
32 the C^* values obtained with different techniques were found to be in good agreement (within 1 order of magnitude) with
33 deviations explained by the different operating conditions of the PTRMS.

34 The C^* of the identified organic compounds were mapped onto the 2-dimensional volatility basis set (2D-VBS) and results
35 showed a decrease of the C^* with increasing oxidation state. For all experiments conducted in this study, identified
36 partitioning organic compounds accounted for 20-30 % of the total organic mass measured from an AMS. Further
37 comparison between observations and theoretical calculations was performed for species found in our experiments that were
38 also identified in previous publications. Theoretical calculations based on the molecular structure of the compounds showed,
39 within the uncertainties ranges, good agreement with the experimental C^* for most SVOCs, while IVOCs deviated up to a
40 factor of 300. These latter differences are discussed in relation to two main processes affecting these systems: (i) possible
41 interferences by thermal and ionic fragmentation of higher molecular weight compounds, produced by accretion and
42 oligomerization reactions, that fragment in the m/z range detected by the PTRMS and (ii) kinetic influences in the
43 distribution between gas- and particle-phase with gas-phase condensation, diffusion in the particle-phase and irreversible
44 uptake.

45 1 Introduction

46 Secondary organic aerosol (SOA), formed by chemical reactions in the atmosphere, constitute a major fraction of the organic
47 aerosol ((OA); Jimenez et al 2009)) and thus play a key role in climate change and air quality. A detailed understanding of
48 SOA formation and composition ~~needs is critical to be well-defined~~ ~~develop strategies~~ for impact mitigation (Volkamer et al.,
49 2006; de Gouw et al., 2008; Hallquist et al., 2009; Jimenez et al., 2009). Defining the fundamental parameters that distribute
50 organic molecules between the gas and particle phases is essential, as atmospheric lifetime and impacts change drastically
51 between phases. The saturation vapor pressure (Pankow, 1994) and the enthalpies of vaporization and sublimation are key
52 thermodynamic properties describing the gas-to-particle partitioning of organic compounds. Since SOA consists
53 predominantly of oxidized multifunctional compounds (McFiggans et al., 2010) they are expected to show low saturation
54 vapor pressures thus increasing the detection challenges due to the low gas-phase concentrations that need to be probed
55 (Bilde et al., 2015).

56 Advanced instrumentation for defining the saturation vapor pressure and thus the volatility of single component and complex
57 organic aerosol systems has been developed in the past decades both for laboratory and field studies. Dicarboxylic acids
58 represent a class of low-volatility compounds commonly found in atmospheric aerosol that are commercially available.
59 These molecules have been extensively studied by various techniques (Bilde et al., 2015). Namely, the Knudsen effusion
60 mass spectrometry (KEMS) (Booth et al., 2009) is a method where macroscopic crystalline samples effuse in a Knudsen cell
61 and the change of the concentration in the gas-phase is measured using a mass spectrometer and translated to saturation
62 vapor pressure values based on calibrated standards. Single particle methods using optical tweezers (Mitchem and Reid,
63 2008) and the electrodynamic balance (EDB) (Pope et al., 2010) infer saturation vapor pressure values from the evaporation
64 or condensational growth of a single particle at a controlled environment. Thermal desorption mass spectrometry (TDMS)
65 has extended the studies from laboratory to ambient complex polydisperse systems. Thermodesorbers have been extensively
66 used to quantify the volatility of the bulk OA (An et al., 2007; Huffman et al., 2008; Faulhaber et al., 2009; Gkatzelis et al.,
67 2016; Louvaris et al., 2017; Isaacman-VanWertz et al., 2017) with the support of model calculations (Riipinen et al.,
68 2010; Karnezi et al., 2014). However, the detector used in most of these studies is an Aerosol Mass Spectrometer (AMS)
69 (Canagaratna et al., 2007) that operates at high vaporizer temperatures (600 °C) and ionizes the analytes by electron impact
70 (70 eV) thus introducing excessive thermal and ionic dissociation.

71 Recently, several different methods have been developed that compromise between molecular level information for a small
72 fraction of the OA mass (Williams et al., 2006; Kreisberg et al., 2009; Hohaus et al., 2010; Williams et al., 2014; Zhang et al.,
73 2014) or chemical formula identification using soft ionization MS to achieve a nearly full OA characterization (Lopez-
74 Hilfiker et al., 2014; Isaacman-VanWertz et al., 2017; Stark et al., 2017; Gkatzelis et al., 2018). Volatility measurements are
75 performed either by calibrating with standards of known saturation vapor pressure (Lopez-Hilfiker et al., 2014; Lopez-
76 Hilfiker et al., 2015) or by simultaneous measurement of the gas- and particle-phase of an ion ~~when applicable~~ (Hohaus et
77 al., 2015; Isaacman-VanWertz et al., 2016; Stark et al., 2017).

78 In order to identify the OA on a molecular level, thermal desorption techniques have been coupled to Gas-Chromatography
79 (GC) methods. The Thermal Desorption Aerosol Gas Chromatograph/Mass Spectrometer (2D-TAG) ~~(Isaacman et al., 2011)~~
80 ~~and the Volatility and Polarity Separator (VAPS) (Martinez et al., 2016) are similar techniques that provide volatility and~~
81 ~~polarity-resolved OA information by using a 2-dimensional gas chromatography (2D-GC) approach. Volatility is derived~~
82 ~~based on the two-dimensional chromatographic retention times relative to those of known standards, thus establishing a~~
83 ~~retention time correlation (RTC) to the vapor pressure. Simultaneous measurements of the gas- and particle-phase mass of~~
84 ~~organic molecules has also been recently developed using the modified semi-volatile TAG (SV-TAG) that utilizes two TAG~~
85 ~~cells in parallel (Isaacman-VanWertz et al., 2016). Although the above GC methods provide chemical speciation and gas-to-~~
86 ~~particle partitioning in a molecular level, they can only do so for a small fraction of the OA mass (10–40 %). (Goldstein et~~
87 ~~al., 2008) and the Volatility and Polarity Separator (VAPS) (Martinez et al., 2016) are similar techniques that provide~~

88 volatility- and polarity-resolved OA information by using a 2-dimensional gas chromatography (2D-GC) approach.
89 Volatility is derived based on the two-dimensional chromatographic retention times relative to those of known standards,
90 thus establishing a retention time correlation (RTC) to the vapor pressure. Simultaneous measurements of the gas- and
91 particle-phase mass of organic molecules has also been recently developed using the TAG system sampling alternately with
92 and without a gas phase denuder in front of the inlet (Zhao et al., 2013b) and the modified semi-volatile TAG (SV-TAG) that
93 utilizes two TAG cells in parallel (Isaacman-VanWertz et al., 2016). Although the above GC methods provide chemical
94 speciation and gas-to-particle partitioning in a molecular level, they can only do so for a small fraction of the OA mass (10 –
95 40 %) (Williams et al., 2006; Williams et al., 2016).
96 Measurements using instrumentation to provide molecular identification (e.g. SV-TAG) or instrumentation for the
97 identification of ions (e.g. different Chemical Ionization Mass Spectrometer (CIMS)) can be combined to increase the
98 understanding of partitioning of some compounds classes. This was shown in an field intercomparison investigating gas-
99 particle partitioning of oxygenated VOCs during the Southern Oxidant and Aerosol Study (SOAS) (Thompson et al., 2017).
100 Newly developed thermal desorption inlets have allowed near-simultaneous chemical characterization of gas- and particle-
101 phase ambient compounds (Holzinger et al., 2010; Lopez-Hilfiker et al., 2014; Yatavelli et al., 2014; Eichler et al., 2015; Stark
102 et al., 2017; Gkatzelis et al., 2018). When coupled to chemical ionization high resolution time-of-flight mass spectrometers
103 (ToF-CIMS) these inlets can provide information on a very broad volatility range (Eichler et al., 2017). By simultaneous
104 measurement of the gas- and particle-phase mass concentration when applicable, direct volatility calculations of individual
105 species can be performed. Indirect ways of estimating the vapor pressure for this type of systems has been also established
106 based on the desorption temperature of calibrated known species or mixtures (Lopez-Hilfiker et al., 2016; Stark et al., 2017).
107 Since the above mass spectrometric techniques can provide elemental formulas, methods to derive the vapor pressure by
108 assuming a functional group composition have also been widely used (Pankow and Asher, 2008; Krechmer et al.,
109 2015; Daumit et al., 2013; Li et al., 2016). A detailed comparison of the three different methods of estimating the vapor
110 pressure for this type of techniques has been performed for field studies under forested areas (Stark et al., 2017). Results
111 suggested that thermal decomposition pathways could bias the direct partitioning calculation based on the gas- and particle-
112 phase concentrations as well as calculations based on the chemical formula of the species detected. Detailed understanding
113 on the decomposition pathways is to be determined in future studies.
114 There are two major ways established in the last years to treat partitioning for practical applications to atmospheric aerosol.
115 One is through a thermodynamic model containing an ensemble of specific molecules while the other is based on empirical
116 calculations (Donahue et al., 2014). When using explicit methods, model systems are treated as fully as possible thus
117 individual vapor pressures and activity coefficients are calculated based on several thermodynamic schemes (Fredenslund et
118 al., 1975; Clegg et al., 2001; Zuend et al., 2011). These calculations are strongly affected by the wide range of vapor pressure
119 estimates from the different theoretical approaches (Camredon et al., 2010; Donahue et al., 2014), thus further promoting the
120 need of future development in this field. On the contrary, empirical methods tend to simulate gas-to-particle partitioning
121 based on fits of partitioning data derived from chamber observations. Frameworks like the 2-Dimensional Volatility Basis
122 Set (2D-VBS) classify OA in terms of bulk chemical characteristics and volatility (Donahue et al., 2013; Donahue et al.,
123 2012). A variety of the above newly developed techniques can be mapped onto the 2D-VBS and thus provide important
124 experimental input to further develop and test both the empirical methods and the newly developed instrumentation.
125 Deviations ~~of~~between the theoretical ~~to~~and experimental vapor pressure estimates are systematically observed (Bilde et al.,
126 2015). Recent measurements show enrichment of semi-volatile organic compounds in the particle- relative to the gas-phase
127 than calculations based on equilibrium vapor pressure would suggest (Zhao et al., 2013a; Hohaus et al., 2015; Isaacman-
128 VanWertz et al., 2016). It is currently unclear whether this is due to (i) uncertainties in the theoretical estimates of vapor
129 pressures, (ii) thermal decomposition pathways affecting the experimental partitioning determination or (iii) the existence of
130 uptake pathways to particles other than absorption e.g. adsorption or reactive uptake. The wide range of theoretical vapor

131 pressure estimates combined with the large gas-to-particle partitioning discrepancies of the above techniques (Thompson et
132 al., 2017) promote further studies in order to bridge the gap between theory and experiments.
133 In this study, the gas-to-particle partitioning of major biogenic SOA (BSOA) oxidation products was investigated. An inter-
134 comparison was performed using three different inlet techniques connected to soft-ionization mass spectrometry, the Aerosol
135 Collection Module (ACM) (Hohaus et al., 2010), the Chemical Analysis of Aerosol Online (CHARON) (Eichler et al., 2015)
136 and the Collection Thermal Desorption Cell (TD) (Holzinger et al., 2010). Volatility measurements were derived based on
137 the mass concentration of individual species in the gas- and particle-phase, implemented in the 2D-VBS and compared to
138 various explicit methods.

139 2 Methods and instrumentation

140 2.1 Facilities

141 The SAPHIR chamber is an atmospheric simulation chamber made of a double walled Teflon (FEP) foil with a volume of
142 270 m³. It has a cylindrical shape and is housed in a steel frame. A shutter system mounted on the steel frame allows ~~to~~
143 ~~conduct~~ experiments to be conducted in the dark or when opened exposes the chamber to natural sunlight to initiate
144 photochemistry. The pressure inside the chamber is kept at about 50 Pa overpressure compared to ambient pressures to
145 ensure no diffusion from trace gases from the outside into the chamber. Additionally, the interspace of the double walled
146 Teflon film is continuously flushed with pure nitrogen (Linde, purity 99.9999 %). A continuous flow of ultra clean air into
147 the chamber compensates any losses due to leakages and ensures stable pressure conditions.

148 In preparation for each experiment the chamber is flushed with a high flow of up to 250 m³/h for several hours using the
149 ultra-clean air. The same high flow rate is used to humidify the chamber before the start of each experiment. For
150 humidification Milli-Q water is boiled and the steam is added to the air stream into the chamber. Two fans mounted inside
151 the chamber generate well mixed starting conditions and were turned off as soon as aerosol production was initiated to reduce
152 aerosol losses in the chamber. Ozone is added using a silent discharge ozonizer. Standard instrumentation is continuously
153 measuring the conditions inside the SAPHIR chamber. Instrumentation includes an ultrasonic anemometer (Metek USA-1,
154 accuracy 0.3 K) to measure the air temperature, a frost point hygrometer (General Eastern model Hygro M4) to determine
155 the humidity, and a chemiluminescence analyser (ECO PHYSICS TR480) equipped with a photolytic converter (ECO
156 PHYSICS PLC760) to measure NO and NO₂. Ozone is measured by an UV absorption spectrometer (ANSYCO model
157 O341M). Further details of the SAPHIR chamber are described in Rohrer et al. (2005).

158 Precursor compounds were added using two separate methods. The first method was to inject pure liquid compounds via a
159 syringe in a heated inlet line, into the air stream with which the vapors were transported into the chamber. The second
160 method was to use the plant chamber SAPHIR-PLUS (Hohaus et al., 2016) to transfer the emissions of six *Pinus sylvestris* L.
161 (scots pine) into the chamber. Injection flow from SAPHIR-PLUS was 6 m³/h which replaced to a large ~~extend~~ extent the
162 flow of clean air (8 m³/h) which is needed to replace air lost due to leakage and withdrawal of analytical instrumentation.
163 The environmental parameters of the plant chamber are fully controlled (e.g., temperature, soil relative humidity,
164 photosynthetically active radiation). The average temperature inside the SAPHIR-PLUS chamber was 25 °C. Details on the
165 SAPHIR-PLUS are provided in Hohaus et al. (2016).

166 2.2 Instrumentation

167 ~~All instruments used in this study are described in detail in Gkatzelis et al. (2017) and only an~~ All instruments used in this
168 study are described in detail in Gkatzelis et al. (2018) and only a brief overview is provided in the following. An Aerodyne
169 High-Resolution Aerosol Mass Spectrometer (HR-AMS) (DeCarlo et al., 2006; Canagaratna et al., 2007) and a Scanning
170 Mobility Particle Sizer (SMPS, TSI Classifier model 3080, TSI DMA 3081, TSI Water CPC 3786), were used to determine

171 the aerosol chemical composition including the total organic mass concentration and the size distribution during the
172 experiments, respectively. In order to determine the saturation mass concentrations (C^*) parallel gas- and particle-phase
173 measurements were performed. Particle-phase composition was measured using three different aerosol sampling techniques
174 coupled to a Proton-Transfer-Reaction Time-of-Flight Mass Spectrometer (model PTR-TOF 8000; PTR-ToF-MS, Ionicon),
175 the Aerosol Collection Module (ACM-PTR-ToF-MS, referred to as “ACM” hereafter) (Hohaus et al., 2010), the chemical
176 analysis of aerosol online (CHARON-PTR-ToF-MS, referred to as “CHARON” hereafter) (Eichler et al., 2015) and the
177 collection thermal desorption unit (TD-PTR-ToF-MS, referred to as “TD” hereafter) (Holzinger et al., 2010). In the
178 following, the most important characteristics and parameters are described briefly ~~and for more details the reader is referred~~
179 ~~to Gkatzelis et al. (2017)~~. The CHARON inlet combines a gas phase denuder, an aerodynamic lens with an inertial sampler
180 and a thermodesorption unit which is coupled to a PTR-ToF-MS. The gas phase denuder removes gas phase analytes.
181 Subsequently the aerosols are collimated by the aerodynamic lens and a particle enriched sample flow is achieved by the
182 inertial sampler. Afterwards the particles pass through a thermal desorption unit in which the particles are volatilized before
183 transferred to the gas phase detector. The ACM has two sample air inlets. For the gas phase inlet air passes through a PTFE
184 particle filter and is then directly introduced into the PTR-MS. For particle collection via the second sampling line air is
185 passing through an aerodynamic lens removing gas phase and collimating particles onto a beam. The particles are
186 subsequently passing a vacuum chamber and are collected on a cooled sampling surface. Once collection is finished particles
187 are desorped and transferred via a carrier gas (N_2) to the PTR-ToF-MS detector. Important to note is that during the
188 collection process the PTR-ToF-MS is measuring the gas phase in parallel allowing for quasi simultaneous characterization
189 of gas and particle phase. The TD also employs a gas phase denuder to remove gas phase analytes before the aerosols are
190 impacted using a Collection and Thermo-Desorption (CTD) cell. After collection particles are thermally desorped and the
191 components transferred to the PTR-ToF-MS. In the following, operational parameters are listed for all PTR-based
192 instruments. The CHARON is a real time measurement (10 s integration time in the detector), while the ACM and TD have
193 sampling times for this study of 120 min and 240 min, respectively. The CHARON inlet was operated at low pressure (< 1
194 atm) and at a constant temperature of 140 °C. The sampling in the ACM was under vacuum conditions and at sub-zero
195 temperature (-5 °C). The sampling in the TD was at ambient temperature and at atmospheric pressure. The CHARON used a
196 gas-phase denuder to strip off gas-phase compounds while the AMS-type vacuum inlet system of the ACM ensured a
197 removal of the gas-phase. While the particle-phase in the CHARON was desorped by passing particles through a
198 thermodenuder, the particle-phase in the ACM and TD was desorped after collection from the collection surface using a
199 temperature ramp reaching a final temperature of 250 °C and 350 °C, respectively. All three aerosol collection techniques are
200 utilizing a PTR-ToF-MS as a detector. The operational conditions for each PTR-ToF-MS were different with regard to a
201 different electric field strength ($V\ cm^{-1}$) to buffer gas density (molecules cm^{-3}) ratio (E/N). This can lead to different ionic
202 fragmentation behavior. Therefore the overlap of parent ions measured between the different instruments can be reduced. A
203 detailed discussion about the E/N effect has been investigated by Gkatzelis et al. (2018). Operational details for the different
204 PTR-ToF-MS conditions are given also in Table S2. The PTR-ToF-MS of the CHARON, ACM, and TD were operated at
205 100 Td, 120 Td, 160 Td, respectively ($1\ Td = 10^{-17}\ V\ cm^2\ molecule^{-1}$). The drift tube conditions for the PTR-ToF-MS of
206 CHARON, ACM, and TD were at a temperature of 100 °C with a pressure of 2.30 mbar, 120 °C and a pressure of 2.40
207 mbar, and 120 °C and a pressure of 2.40 mbar, respectively. The limit of detection (LOD), depended on the different pre-
208 concentration factors for each technique, which resulted in TD having the lowest LOD ($10^{-3}\ ng\ m^{-3}$), followed by the
209 CHARON ($1.4\ ng\ m^{-3}$), while ACM showed the highest values ($250\ ng\ m^{-3}$). Finally, differences in sensitivity for each
210 PTR-MS introduced minor deviations in this study and are discussed in detail in Gkatzelis et al., (2018). A characteristic
211 timeseries of a major oxidation product from the β -pinene ozonolysis for the three different techniques can be found in
212 Figure S8.

213 Gas-phase organic compounds were detected by a standalone PTR-ToF-MS for the CHARON and TD. The standalone PTR-
214 ToF-MS was operated with an E/N = 120 Td. The drift tube was kept at a temperature of 60 °C and a pressure of 2.30 mbar.
215 The standalone PTR-MS was connected to SAPHIR via a 0.5 m PFA line (inner diameter, i.d. 3.2 mm), to a 2 m PEEK line
216 (i.d. 1 mm), heated at 60 °C with a flow of 0.6 L min⁻¹ that resulted to an overall residence time of ~ 0.6 s. The ACM was
217 connected via a 4 m PFA line (i.d. 4 mm), at room temperature with a flow of 0.7 L min⁻¹, resulting to a residence time of
218 approximately 3 s. A PTFE particle filter (Merck Millipore) was additionally introduced to the PTR-MS line of the ACM to
219 reassure complete particle-phase removal. Gas-phase compounds were then directed to the ACM-PTR-MS interface that was
220 heated at 280 °C via a 5 cm coated stainless steel line (i.d. 0.8 mm) to the PTR-MS. The ACM design allowed for
221 simultaneous gas-phase measurements with the same PTR-ToF-MS while sampling of the particle-phase took place on the
222 ACM collector. Comparison of gas and particle-phase measurements was thus performed using the same detector avoiding
223 any detector related differences. It should be noted that TD and CHARON are also designed for simultaneous gas- and
224 particle-phase measurements using the same PTR-MS but in this study this feature was not operational.

225 2.3 Experimental conditions

226 Before each experiment the SAPHIR chamber was flushed with clean air over night (total volume exchange was about 2000
227 m³) and humidified directly after the flushing process. Relative humidity (RH) in the chamber was about 55 % within a
228 temperature range for all experiments between 295 K and 310 K. After ensuring that all instruments had measured the
229 background in the SAPHIR chamber a single monoterpene (β -pinene or limonene), a monoterpene mixture (β -pinene and
230 limonene) or the emissions of 6 *Pinus sylvestris* L. (Scots pine) were injected. The tree emissions were characterized using
231 GC-MS. The composition of the biogenic VOC (BVOC) consisted of 42% δ 3-carene, 38% α -pinene, 5% β -pinene, 4%
232 myrcene, 3% terpinolene and 8% other monoterpenes. The details of all experiments are given in Table 1 and an
233 experimental overview is provided in Figure S1. One hour after injection of the VOCs ozone was introduced into the
234 chamber to initiate ozonolysis with the subsequent formation of secondary organic aerosols (SOA). Experiments were done
235 without the use of an OH scavenger. NO_x concentrations during the experiments ranged between 10 to 60 pptVpptv
236 originating from HONO background source (Rohrer et al., 2005). In all experiments, except for the experiment with
237 limonene as a precursor, 20 hours after the start of the ozonolysis the roof of the SAPHIR chamber was opened to initiate
238 additionally additional photochemistry with OH and ageing of the SOA. For the limonene experiment instead of opening the
239 roof, 30 ppbVppbv of NO was added to the chamber. With the remaining ozone in the chamber, NO₃ oxidation was initiated.
240 In the tree emissions experiment the SAPHIR-PLUS chamber was recoupled to the SAPHIR chamber 11 hours after the start
241 of the ozonolysis thus injecting again fresh BVOC emissions from the scots pines. The experiment continued for an
242 additional 6 hours with the roof open allowing for further oxidation of the BVOCs and SOA by OH radicals. The duration of
243 the experiments varied from 17 to 36 hours, providing ample time to experimentally investigate the aging of the biogenic
244 SOA.

246 2.4 Estimation of volatility distribution

247 In this work the volatility of different species was quantified based on their saturation mass concentration C* in units of
248 $\mu\text{g m}^{-3}$. Theoretical calculation of the saturation concentration was performed for known oxidation products of the
249 monoterpenes studied based on their chemical structure as seen in Table S1. Based on the absorption equilibrium partitioning
250 formalism, the (sub-cooled liquid) saturation vapor pressure ($p_{i,l}$) of a species was related to its C* based on Cappa and
251 Jimenez (2010) Based on the absorption equilibrium partitioning formalism, the (sub-cooled liquid) saturation vapor pressure
252 ($p_{i,l}$) of a species was related to its C* based on Cappa and Jimenez (2010) as following:

$$C^*(T) = \frac{MW_i \times 10^6 \times p_{iL} \times \zeta_i}{R \times T} \times \frac{MW_{OA} \times 10^6 \times p_{iL} \times \zeta_i}{R \times T} \quad (1)$$

where MW_i, MW_{OA} is the molecular weight of ~~a compound in the condensed organic phase~~ (g mol⁻¹), $p_{i,L}$ is the sub-cooled liquid saturation vapor pressure (Pa), ζ_i is the activity coefficient of species i in the OA phase, T is the chamber temperature (K) and R is the ideal gas constant (8.314 J mol⁻¹ K⁻¹). Here, the calculations were performed using a mean molecular weight of 180 g mol⁻¹ (Prisle et al., 2010). In conformity with Donahue et al. (2014) the activity coefficients of all considered species partitioning into a mixed aerosol system containing similar compounds were assumed to be 1 throughout the study. At present, there is a scarcity of reliable saturation vapor pressure data obtained through laboratory studies (Bilde et al., 2015). Therefore, $p_{i,L}$ is commonly estimated using empirical relationships derived from the Clausius-Clapeyron equation e.g. (Myrdal and Yalkowsky, 1997; Jenkin, 2004; Nannoolal et al., 2008). The required thermodynamic properties, such as the boiling temperature or the enthalpy of vaporization are predicted from the molecular structure of the investigated compounds (Mackay et al., 1982; Joback and Reid, 1987; Stein and Brown, 1994). Their explicit manual calculation using the existing functional group contribution methods are very laborious not only because of the high number of components, but also because of the wide range of multifunctional organic compounds in the aerosol mixtures. Recently, a new web-based facility, UManSysProp (<http://umansysprop.seaes.manchester.ac.uk>), was developed for automating predictions of i.e. pure component vapor pressures of organic molecules or activity coefficients for mixed liquid systems. For the group contribution approaches, only the molecular information must be uploaded in form of SMILES (Simplified Molecular Input Line Entry System) strings (Toppings et al., 2016). At a defined temperature, there are several options for vapor pressure predictive techniques, providing the possibility to combine two different empirical representations of the Clausius-Clapeyron equation (Myrdal and Yalkowsky, 1997; Nannoolal et al., 2008) - further referred to as MY and NN, respectively - with three different prediction methods for thermodynamic properties of the investigated compound based on their molecular structure (Joback and Reid, 1987; Stein and Brown, 1994; Nannoolal et al., 2008) - further referred to as JR, NN and SB, respectively. Additionally, the EVAPORATION method (further referred to as EVAP) proposed by Compernelle et al. (2010) is available for the web-based calculations.

Here, we use the $p_{i,L}$ predicted online by UManSysProp facility, examining all seven estimation methods (Figure S6 and S7). Only the results giving the lowest and highest vapor pressures for the studied compounds (the range of the estimates are indicated by the grey background color) are used in this study to compare measurements to the highest and lowest possible theoretical values.

~~Experimental determination of the saturation mass concentration of the individual compounds was derived by applying the partitioning theory (Pankow, 1994) based on Donahue et al. (2006) as~~
~~Experimental determination of the saturation mass concentration of the individual compounds was derived by applying the partitioning theory (Pankow, 1994) based on Donahue et al. (2006) as~~

$$C^* = OA \times \frac{G_i}{P_i} \quad (2)$$

where OA is the total organic mass ($\mu\text{g m}^{-3}$) determined from AMS and G_i and P_i are the gas- and particle-phase mass concentration ($\mu\text{g m}^{-3}$) of compound i , respectively, measured from the PTR based techniques. Assuming typical vaporization enthalpies (Epstein et al., 2010) (e.g. $\Delta H^{\text{VAP}} = 127 \text{ kJ mol}^{-1}$) (Epstein et al., 2010), C^* and therefore partitioning is strongly dependent on temperature with changes of $\pm 15 \text{ }^\circ\text{C}$ resulting in a C^* change by a factor of $\pm 10 \mu\text{g m}^{-3}$. During the campaign the average chamber temperatures and their standard deviations were $20 \pm 4 \text{ }^\circ\text{C}$, $17 \pm 4 \text{ }^\circ\text{C}$, $19 \pm 5 \text{ }^\circ\text{C}$ and $30 \pm 5 \text{ }^\circ\text{C}$ for the β -pinene, limonene, mixture and trees experiment, respectively. ~~Nevertheless, these variations ($< 10 \text{ }^\circ\text{C}$) can be considered small. The uncertainty added from these variations ($< 10 \text{ }^\circ\text{C}$) was further examined with a focus on the β -pinene oxidation products (Figure S7). Difference in volatility due to variations ranged from 0.3 to 0.6 log(C^*) depending on the chemical structure of the compound. Nevertheless, these variations can be considered small and not strongly affecting the~~

Formatiert: Schriftartfarbe:
Automatisch

295 [conclusions of this work](#). Therefore, for consistency with other studies, a reference temperature of 298 K was used
296 throughout all C^* calculations. This was recently proposed by Stark et al. (2017) to derive the average C^* for the
297 BEACHON and SOAS field campaigns making the assumption that deviations due to temperature changes (18 ± 7 °C and
298 25 ± 3 °C, respectively) were within the uncertainties of the measurements. [Calculation of the average \$C^*\$ for each](#)
299 [experiment was performed based on the time resolution of each instrument \(section 2.2\). When the signal in the particle-](#)
300 [phase was close to the detection limit, introducing a high uncertainty, the calculation of the \$C^*\$ was not performed.](#)
301

302 3 Results and discussion

303 3.1 Compound selection: Assessment of ionic and thermal decomposition

304 For all PTR based techniques the molecular formula $(C_xH_yO_zN_a)H^+$ was attributed to each detected signal derived from the
305 exact molecular mass which was determined by the TOF-MS. Whether the detected ion was an original SOA compound or a
306 fragment detected on this mass could be affected by two major processes, (i) thermal dissociation during desorption, and (ii)
307 ionic dissociation in the ionization region of the PTR-ToF-MS.

308 Thermal dissociation has been found to introduce a high degree of fragmentation for compounds that contain multiple
309 functional groups, including peroxide groups which are thermally labile (Lopez-Hilfiker et al., 2015). For organic alcohols
310 and acids thermal desorption has been shown to lead to loss of carboxyl- ($-CO_2$), carbonyl- ($-CO$) and water-groups ($-H_2O$)
311 (Canagaratna et al., 2015). Accretion reactions and gas-phase autoxidation have been found to play a key role in extremely
312 low volatility OC (ELVOC) formation (Tobias and Ziemann, 1999, 2001; Ehn et al., 2014). Upon heating, such products will
313 thermally decompose (Barsanti et al., 2017) and be detected in the lower molecular weight range, thus directly affecting the
314 partitioning estimation (Jang and Kamens, 2001; Stark et al., 2017). All instruments deployed in this study were subjected to
315 possible thermal dissociation with decarboxylation and dehydration reactions strongly dependent on the temperature,
316 pressure and the heat exposure time of the molecules during desorption. CHARON was operated at the lowest temperature of
317 140 °C, under a few mbars of pressure and with the lowest heat exposure time, therefore minimizing the latter reactions.
318 ACM and TD were operated at 1 bar and up to 250 °C and 350 °C, respectively, with longer heat exposure times.

319 Functional group loss has been found to additionally occur in the ionization region of the PTR-ToF-MS instruments.
320 Gkatzelis et al. (2018) showed that for this study the ratio of the electric field strength ($V\text{ cm}^{-1}$) to buffer gas
321 density (molecules cm^{-3}) (E/N) in the PTR-ToF-MS instruments played a key role in decomposition, not only due to water
322 loss but also carbon-oxygen bond breakage of the detected molecules. Even though PTRMS is considered a soft ionization
323 technique compared to e.g. AMS, these decomposition pathways could still lead to misidentification of the original chemical
324 composition of the SOA species. For the ACM the ionic fragmentation for the gas- and particle-phase species was identical
325 since both measurement were conducted using the same PTR-ToF-MS as a detector. CHARON and TD saturation mass
326 concentration (C^*) was determined by using the gas-phase mass concentration measurements derived from a separately
327 deployed PTR-ToF-MS operated at different E/N conditions (see Section 2.2). Ionic dissociation was thus different for the
328 gas- compared to the particle-phase measurements increasing the uncertainty of the volatility estimation for CHARON and
329 TD when compared to ACM.

330 A method to identify the ionic and thermal dissociation processes and their effect to the different techniques is presented in
331 the following. This method was applied to the calculated average $\log(C^*)$ of each ion, found both in the gas- and particle-
332 phase, for each experiment for the individual instruments. A characteristic example of the β -pinene ozonolysis experiment
333 (as shown in Figure 1) for the ACM is used here to explain this method. Information of the carbon (x-axis) and oxygen (size
334 of the markers) atom number contained in the chemical formulas were used to differentiate between the different ions
335 (Figure 1a). Each marker indicates one ion, therefore for the β -pinene experiment 72 ions were detected both in the gas- and

336 particle-phase by the ACM. Their average saturation mass concentration $\log(C^*)$ and therefore their volatility ranged from
337 10^1 to $4 \cdot 10^4 \mu\text{g m}^{-3}$, an indication of semi-volatile and intermediate-volatile species in the SOA mass. From these ions, 55
338 were identified as fragmentation products accounting for 70 % of the partitioning ions and only 25 % of these ions were used
339 for further analysis.

340 Two major criteria were applied to differentiate between a possible parent ion (green markers) and a fragment. The first
341 criteria was if the carbon and oxygen atom number were lower than 6 and 1, respectively. ~~This criteria was chosen based on~~
342 ~~Donahue et al. (2006)~~ This criteria was chosen based on Donahue et al. (2006) who have shown that organic aerosols are
343 expected in the range from ELVOC to SVOC and IVOC with saturation concentrations ranging from -5 to 4. This volatility
344 regime consists of species with carbon and oxygen atom numbers equal or larger than 6 and 1, respectively (Donahue et al.,
345 2012; Donahue et al., 2011). Ions found in the particle-phase with lower carbon and oxygen numbers were thus considered
346 fragmentation products (grey markers) and were not used in the analysis. The second criteria focused on the dependence of
347 the volatility to the number of oxygen and carbon atoms that constitute an organic molecule. As the oxygen and carbon atom
348 number and thus the functionality of the molecule increased, the saturation mass concentration was expected to decrease
349 (Pankow and Barsanti, 2009). If the volatility of an identified ion $[M+H]^+$ was identical to (within an uncertainty of
350 $\log(C^*) \pm 0.25$) or higher than the volatility of ions with the same chemical formula subtracting a functional group $[M+H-$
351 $FG]^+$ the latter were considered highly affected by either ionic or thermal dissociation and were excluded from further
352 analysis. Characteristic examples of this analysis are shown in Figure 1b and c. The y-axis corresponded to identified ions
353 $[M+H]^+$ while the x-axis to ions with the same chemical formula subtracting water ($-H_2O$) (Figure 1b) or a carbonyl group ($-$
354 CO) (Figure 1c). When the ions $[M+H]^+$ and $[M+H-FG]^+$ were found to have identical saturation concentrations, $[M+H-FG]^+$
355 ions were excluded (blue and orange markers in Figure 1b and c, respectively). $[M+H-FG]^+$ ions that showed lower volatility
356 when compared to $[M+H]^+$ ions were considered fragments of unknown decomposition pathways (i.e. unknown parent ion
357 composition) and were excluded as well (yellow markers). Only when ions $[M+H-FG]^+$ showed higher volatility values than
358 $[M+H]^+$ they were considered to be possible parent ions not strongly affected by thermal or ionic dissociation (green
359 markers) and were further analyzed. The same comparison was not only performed for ($-H_2O$) and ($-CO$) functional group
360 loss but was extended to ($-CO_2$), ($-H_2O_2$), ($-H_2O$) plus ($-CO$), and ($-H_2O$) plus ($-CO_2$). ~~It should be noted~~ Checks were also
361 performed for loss of the ($-HNO_3$) functional group for the limonene- NO_3 oxidation experiment but due to the high E/N
362 operating conditions of all PTR-ToF-MS systems, no organic nitrates were identified (Duncan et al., 2017).

363 ~~It should be noted that PTR-MS provides information regarding the chemical formula of an ion and thus disregards potential~~
364 ~~impact of the chemical structure. Functionality effect (e.g. stronger hydrogen bonding of an alcohol in a polar particle) can~~
365 ~~lead to a misidentification of potential parent ions as a fragment using the above described method due to the fact that a~~
366 ~~lower volatility is determined compared to an expected volatility based on the chemical formula. Nevertheless, although this~~
367 ~~method will potentially exclude parent ions, it will still discard also any possible fragments. Correlation analysis based on~~
368 ~~the time series of the different compounds could further improve the parent ion identification. However due to the low time~~
369 ~~resolution in this work a time series analysis is not applicable. Another implication relies on the fact that $[M+H]^+$ ions could~~
370 result from the decomposition of accretion reaction products or oligomers, consequently leading to an overestimation of their
371 particulate phase concentrations. This effect is not constrained by this method and is further addressed in Section 0.
372 Furthermore, although this method can efficiently eliminate possible fragments it does not provide proof that these fragments
373 originate from the suggested fragmentation pathways. An overview of the fragmentation identification results of this method
374 for each instrument and experiment are provided in Figure S2. Percentages are derived based on the total number of
375 fragment ions and how they distribute (%) to the different fragmentation pathways. For all PTR based techniques 40 to 60%
376 of the partitioning ions were detected below the carbon and oxygen atom number threshold of C6 and O1 respectively. From
377 the remaining species, ions affected by water ($-H_2O$) loss were around 5-10%, while carboxyl group ($-CO_2$) fragmentation
378 was identified for less than 10% of the partitioning ions. Loss of ($-CO$), ($-H_2O_2$), ($-H_2O$) plus ($-CO$) and ($-H_2O$) plus ($-CO_2$)

Formatiert: Englisch (Großbritannien)

379 functional groups affected less than 5% of the ions for all experiments and instruments studied. Ions of unknown
380 decomposition pathways represented $\leq 10\%$ with TD showing the highest values. ACM showed increased contributions of
381 lower molecular weight ions, compared to TD and CHARON, for limonene and mixture experiments (max 65%). In total,
382 the fraction of ions identified as parent compounds partitioning in the gas- and particle-phase that were chosen for further
383 analysis in the next sections ranged between 20-40% of the overall ions found in both phases, for each experiment and
384 instrument studied.

385 The high contribution of lower MW ions found both in the gas- and particle-phase for all PTR-based techniques further
386 ~~promoted~~^{supported} that ionic and thermal dissociation played a key role in carbon-oxygen bond breakage. The higher E/N
387 values of ACM and TD compared to CHARON resulted in higher fragmentation, thus higher contribution of the lower MW
388 partitioning ions (Gkatzelis et al., 2017)(Gkatzelis et al., 2018). Although ACM was operated at lower E/N conditions
389 compared to TD, the contribution of lower MW ions was higher. The reason for this discrepancy was due to the higher limit
390 of detection of the ACM (section 2.2) compared to TD and CHARON. Ions of low concentrations in the higher MW range
391 that could be detected from CHARON and TD were below the detection limits of the ACM and were therefore not
392 identified. For the remaining higher MW species, the water (-H₂O) loss was the dominant fragmentation pathway for all
393 techniques. Although the PTR-based techniques were operated at different temperature, desorption residence times and
394 pressure conditions they showed similar ~~percent~~^{percentage} of ions affected by water loss. This is an indication that for all
395 techniques dehydration occurred mostly due to ionic fragmentation in the ionization region of the PTRMS and not due to
396 thermally initiated reactions for the partitioning ions studied. TD showed a higher contribution of fragments of unknown
397 decomposition pathways when compared to ACM and CHARON due to the highest difference of E/N operating conditions
398 in the particle-phase (160 Td) compared to the gas-phase (120 Td), with the latter measured by a separately deployed PTR-
399 ToF-MS. The higher ionic dissociation in the particle-phase increased the concentration of lower MW ions and decreased
400 that of higher MW ions. This had a direct effect on the calculation of the volatility based on equation 2. When this effect was
401 strong enough fragment ions [M+H-FG]⁺ showed higher concentrations in the particle phase thus lower volatility when
402 compared to possible parent ions [M+H]⁺. These ions were, based on this method, excluded as fragments of unknown
403 fragmentation pathways and showed an expected higher contribution for systems like the TD. Fragment loss of (-CO₂), (-
404 CO), (-H₂O₂), (-H₂O) plus (-CO) and (-H₂O) plus (-CO₂) accounted for 10% or less suggesting that these pathways were not
405 dominating the partitioning ions studied. Interference of accretion reaction products or oligomers which could be detected at
406 a lower m/z due to decomposition processes are not accounted for in the ~~preecious~~^{previous} described method. Possible effect
407 of such an interference is further discussed in Section 3.4.

408

409 3.2 Volatility distribution coverage

410 The mass concentrations of only the species identified as parent ions for ACM, CHARON and TD were distributed to
411 different volatility bins ranging from log(C*) of -1 to 5 with a 0.5 ~~bin~~^{bin} volatility resolution. The normalized volatility
412 distribution (NVD) for each experiment accounting for all PTR-based techniques is shown in Figure 2 (1a, 2a, 3a, 4aa, b, c,
413 d). Normalization was performed by dividing each volatility bin by the sum of the PTR-based technique mass concentration
414 measured at each experiment. The detected biogenic SOA partitioning species showed log(C*) values from 0 to 4, an
415 indication that mainly SVOCs and IVOCs were predominantly measured simultaneously in the gas- and the particle-phase.
416 The limonene NO₃ oxidation experiment had the lowest NVD starting from a log(C*) of 0.5, with a narrow spread up to 2.
417 For the β -pinene and β -pinene/limonene mixture experiments the NVD moved towards more volatile species ranging from
418 0.5 to 4. When comparing the single compound experiment of β -pinene to the mixture, the latter showed a NVD shifted to
419 lower saturation concentrations. Partitioning species detected from all the PTR-based techniques were further compared as
420 seen in Figure 2 (1b, 2b, 3b, 4bc, f, g, h). ACM and CHARON showed same volatility values for all experiments with only

421 the trees experiment resulting in higher deviations from the one to one line. TD presented higher $\log(C^*)$ when compared to
422 CHARON and ACM, suggesting the examined species were underestimated in the particle-phase. A total of 5, 2, 6 and 4
423 ions were observed to partition with all three techniques for the β -pinene, limonene, β -pinene/limonene mixture and tree
424 emissions experiment, respectively after applying the parent ion identification method of section 3.1.

425 Calculation of the $\log(C^*)$ in this study relied on the ratio between the gas- and particle-phase signal of an ion (equation 2).
426 Detection limits of both of these limited the measurable range of this ratio. This explains the narrow volatility distributions
427 available with all PTR-based techniques, as has been previously reported by [Stark et al. \(2017\)](#); [Stark et al. \(2017\)](#).

428 Combining the capabilities of these instruments and the above approach to calculate the volatility provided insights in a
429 defined range of SVOCs and IVOCs. Within this volatility range the differences observed when using different precursors
430 agrees with bulk volatility measurement findings that limonene SOA is less volatile than β -pinene SOA (Lee et al., 2011).

431 When focusing on the species measured differences of ACM and CHARON to TD could be explained by the higher E/N
432 conditions of TD that were previously discussed (section 3.1). Since TD was more prone to particle-phase fragmentation
433 compared to the gas-phase these higher MW compounds showed lower concentrations, thus indicated higher volatility. This

434 effect was negligible for ACM that was using the same PTRMS for gas- and particle-phase measurements and lower for
435 CHARON operated at lower E/N conditions. The agreement of ACM and CHARON for all experiments except the trees
436 experiment further promoted that both techniques measured the same species in good agreement and within the uncertainties

437 of these calculations. As the complexity of the system increased, this agreement deviated from the one to one line. Gkatzelis
438 et al. (2018) reported that for the single precursor and mixture experiments ions were detected with C6 to C12 carbon atoms

439 from all techniques. On the contrary, during the tree emissions experiment CHARON was the only instrument to detect ions
440 in the C13 to C20 range. These ions were not detected from ACM or TD that were operated at higher E/N conditions and
441 were more prone to ionic and thermal dissociation. Fragmentation of these higher carbon atom ions could affect the volatility

442 calculation of lower MW species still detected by ACM and TD and thus explain the deviations seen for the tree emissions
443 experiment.

444 The total number of species seen from all techniques was low due to the parent ion identification method applied in the
445 previous section. An overview of the overlapping compounds is provided in Figure S3. When all detected ions were taken
446 into account more than 50 ions were seen from all techniques at each experiment. After narrowing our focus on the
447 partitioning ions and excluding the lower MW fragments the overlapping compounds dropped to ~ 15 ions. Each technique

448 was affected differently by ionic and thermal dissociation. By applying the above method to each technique, different ions
449 were excluded for each instrument thus leading to only a few species seen from all three techniques and accounted as parent
450 ions.

452 3.3 Experimentally derived saturation concentration implemented to the 2D-VBS

453 Species identified as parent ions from each technique were combined and further analysed with a focus on their average
454 saturation concentration as seen in Figure 3. For parent ions measured from more than one instrument, the average of all
455 techniques was used to determine the overall experimental C^* of the ion, with the error bars indicating the error of this

456 average. The 2D-VBS (Murphy et al., 2012; Donahue et al., 2011) framework was used to implement the results for each
457 experiment with background colors corresponding to the different volatility classes, ranging from IVOCs (grey) to SVOCs
458 (green) and LVOCs (red). It should be noted that the oxidation state (OS_{OS_c}) was not derived by bulk measurements using

459 e.g. the AMS, but by using the OS_{OS_c} of the individual species based on their carbon, hydrogen and oxygen atom number
460 (Kroll, 2011). In total 48, 31, 46 and 79 ions were identified as parent ions for the β -pinene, limonene, β -pinene/limonene
461 mixture and tree emissions oxidation experiment, respectively. The saturation concentration showed a decrease for species

462 with higher OS and oxygen atom number. For the limonene experiment lower saturation concentration values for compounds

463 defined by the same oxidation state was found when compared to the β -pinene, mixture or tree emissions experiment.
464 Overall, parent ions corresponded to 20-30 % of the overall organic mass measured from an AMS for all systems studied.
465 The observed volatility decrease with increasing OS and oxygen atom number is in good agreement with previous findings
466 (Jimenez et al., 2009;Kroll, 2011). Lower volatility values for limonene species with the same OS when compared to the β -
467 pinene, mixture or the tree emissions experiment suggested that species originating from different precursors and oxidation
468 pathways with differences in their functionality and molecular structure affected their gas-to-particle partitioning. It should
469 be noted that the lower volatility of limonene could be partly explained by the absence of TD measurement in this
470 experiment and thus the absence of TD C* values when averaging the experimental results from all PTR-based techniques.
471 Since TD was affected the strongest by ionic dissociation (highest E/N), the C* values were biased to higher volatilities
472 when compared to ACM and CHARON with particle-phase measurements (P_i in equation 2) fragmenting more compared to
473 the gas-phase (G_i from dedicated gas-phase PTR operated at lower E/N). Results when averaging all experiments and
474 excluding the TD data are shown in Figure S4. Although the limonene experiment would still show lower volatilities
475 compared to the β -pinene and mixture experiments this trend would be less strong suggesting that the absence of TD during
476 the limonene experiment did lower the overall average volatility calculation presented in Figure 3. The increased number of
477 species detected during the tree emissions experiment occurred due to the higher complexity of this system with more than
478 one precursor oxidized to form SOA. In total, the PTR-based techniques showed that 20-30 % of the overall BSOA mass
479 consisted of ~~compounds~~ions with volatilities within the SVOC to IVOC range further showing the importance of
480 understanding the gas-to-particle partitioning and thermodynamic properties of compounds formed in such systems.
481 At this point, it should be noted that losses of gas-phase compounds through the lines, from the SAPHIR to the PTR-MS,
482 could also affect the $\log(C^*)$ calculation, by changing the ratio of the gas- to the particle-phase. Gas-phase measurements
483 were performed using a standalone PTR-MS for TD and CHARON while for the ACM both gas- and particle-phase
484 measurements were obtained using the same PTR-MS of ACM. The two PTR-MS differed in inlet length, temperature, and
485 material with ACM-PTR-MS introducing higher residence times, thus longer exposure of the gas-phase compounds to the
486 line walls (see Section 2.2). If significant losses of gas-phase compounds in the ACM-PTR-MS compared to the standalone
487 PTR-MS line would occur, the gas-phase concentration would be underestimated and therefore also the $\log(C^*)$ derived by
488 the ACM measurements. To test if the dissimilarities between the different PTR-MS inlet lines are biasing the results of the
489 ACM, re-calculation of the $\log(C^*)$ was performed by using equation 2 and applying the ACM particle-phase concentration
490 (P_i), but changing the gas-phase concentration (G_i) to measurements from the standalone PTR-MS. This calculation was
491 performed for all ions identified as parent ions for the ACM when using the parent ion identification method. An overview
492 of the correlation of the $\log(C^*)$ using the two different gas-phase datasets is shown in Figure S5. For all experiments and for
493 most of the compounds, agreement within the uncertainty of the measurements was found. For the tree emissions oxidation
494 experiment the fraction of compounds deviating from the one to one line was higher. The spread in the data around the one
495 to one line can be explained by the fact that though both PTR-MS were the same ~~model differences in the design e.g. the~~
496 ~~TOF interface existed. These differences introduced additional fragmentation and affected the resolution of the PTR-MS~~
497 ~~(Gkatzelis et al., 2017) and could therefore explain the deviations observed.type of model differences in the e.g. the TOF~~
498 ~~interface and the drift tube. These differences affected the fragmentation and resolution of the PTR-MS (Gkatzelis et al.,~~
499 ~~2018) and could therefore explain the deviations observed. Moreover, the tree emissions experiment showed the highest~~
500 ~~complexity in comparison to the single precursor oxidation experiments, with detected ions that had up to 20 carbon atoms in~~
501 ~~the particles. These higher molecular weight ions fragmented differently when passing through the differing ToF interfaces~~
502 ~~and thus resulted to the observed higher deviation.~~ However the differences are within the experimental uncertainties and
503 therefore no significant bias due to potential inlet line interference could be determined.
504

505 3.4 Experimentally derived saturation concentration compared to explicit methods

506 In order to derive further information from the experimentally determined parent ions, comparison to previous publications
507 was performed for the major oxidation products from (a) the β -pinene ozonolysis (Yu et al., 1999; Jenkin, 2004; Chen and
508 Griffin, 2005; Steitz, 2010; Kahnt, 2012; Hohaus et al., 2015), (b) limonene ozonolysis and NO_3 oxidation (Chen and Griffin,
509 2005; Leungsakul et al., 2005b; Leungsakul et al., 2005a; Jaoui et al., 2006; Kundu et al., 2012) and (c) tree emissions
510 ozonolysis with α -pinene and Δ^3 -carene being the major reactants (Yu et al., 1999; Chen and Griffin, 2005; Praplan et al.,
511 2014). ~~Species detected as. By attributing a chemical structure to the ions identified by the PTR-MS, detected~~ parent ions
512 that overlapped with compounds from previous publications were further examined based on their structural information. An
513 overview of the overlapping compounds and their suggested structures are given in Table S1. Uncertainties introduced by
514 assigning a chemical structure to an ion of a given chemical formula are further discussed in this section.
515 A detailed analysis of the β -pinene ozonolysis experiment was performed as seen in Figure 4. Experimental calculation of
516 the saturation concentration was performed based on the average C^* values throughout the experiment when taking into
517 account all PTR-based techniques with the error bars indicating the $\pm 1\sigma$ of this averaging. The theoretical calculations by
518 UManSysProp facility showed that the combinations of the boiling temperature (T_B) prediction using NN with the $p_{i,L}$
519 empirical expressions using MY yielded the maximum C^* values while T_B by JB with $p_{i,L}$ by NN yielded the minimum C^*
520 values (Figure S6). ~~The method originally proposed by Joback and Reid, 1987 to predict boiling points based on the~~
521 ~~molecular structure of the investigated compounds explicitly treats ring increments, which are relevant to monoterpene~~
522 ~~calculations and thus for this study. Nannoolal et al., 2004 extended the investigated range of functional groups,~~
523 ~~simultaneously introducing information on a greater neighborhood of the central atom of the investigated functional group.~~
524 ~~The T_B function fitted to the chosen experimental dataset enlarged as well yielded lower boiling points for the compounds~~
525 ~~investigated here, associated with higher vapor pressure. The method developed by Myrdal and Yalkowsky, 1997 includes~~
526 ~~heat capacity changes for phase transitions into their empirical representation, yielding a lowering in the vapor pressure~~
527 ~~estimates, compared with the approaches used hitherto (Camredon et al., 2010). The dependency of ΔC_p upon molecular~~
528 ~~flexibility, i.e. the number of torsional bonds (nonterminal sp^3 - and sp^2 , rings), makes this inclusion very interesting for~~
529 ~~monoterpene calculations. Nannoolal et al., 2008 accounted for the heat capacity changes upon vaporization, too. The new~~
530 ~~feature here is that non-additive interaction contribution of multi-functional groups (e.g OH-ketone) are adopted, resulting in~~
531 ~~lower vapor pressure values compared with the previous methods. Higher electron delocalization induce stronger dispersive~~
532 ~~forces, thus decreasing the $p_{i,L}$. This might explain the larger discrepancy between the vapor pressure values calculated by~~
533 ~~NN/MY and JB/NN with the increasing of alcohol/carbonyl/carboxyl functional group number yielded the minimum C^*~~
534 ~~values (Figure S6 and S7). More details regarding the theoretical calculations are provided in the Supplement. The methods~~
535 with the smallest and largest C^* values for the given compounds were chosen to represent the upper and lower limits of the
536 possible theoretical values, when comparing to the observed ones. These limits are expressed in Figure 4 by the error bars on
537 the x-axis with the marker points corresponding to their average. In total, 10 compounds were identified from previous
538 publications to overlap with experimentally detected parent ions for the β -pinene ozonolysis experiment. For most of these
539 compounds theoretical and experimental values agreed within the uncertainties. No significant discrepancies were found for
540 compounds in the SVOC volatility range. However, compounds in the IVOC range were underestimated from the
541 experimental approaches when compared to theory. A characteristic IVOC 1st generation product from the β -pinene
542 ozonolysis is nopinone that has been previously experimentally studied with a focus on the gas-to-particle partitioning
543 (Steitz, 2010; Kahnt, 2012; Hohaus et al., 2015). Comparison of this work to previous studies was performed as it can be seen
544 in Figure 4(a). The results showed agreement of the C^* within $\pm 10^{0.5}$ between the experimental approaches while the theory
545 showed differences of 10^3 in the C^* estimation. This comparison was extended to oxonopinone, being the second

546 underestimated IVOC 1st generation product, where again this study ($\log(C^*) = 3.16 \pm 0.13$) was in good agreement to
547 | Hohaus et al. (2015) ($\log(C^*) = 3.16 \pm 0.12$) using GC-MS but the same sampling technique.

548 To better understand the differences of the experimental to the theoretical approaches, focus was given on the potential
549 sources of uncertainties within both calculations. For the theoretical approach, the more complex the molecules with
550 increasing functional groups were, the higher the uncertainty of the saturation vapor pressure and thus the volatility was.
551 This is depicted by the higher error bars when moving towards SVOCs. First generation products like nopinone are not
552 characterized by high complexity, thus theory provided more reliable thermodynamic values also reflected by the good
553 | agreement between all theoretical approaches (Figure S6 and S7). The experimental calculation of the volatility
554 performed by the PTR-based techniques could be affected by the (i) existence of isomers within a studied m/z with different
555 structural information and thus thermodynamic properties, (ii) thermal and ionic fragmentation of higher molecular weight
556 compounds, produced by accretion and oligomerization reactions, down to the m/z detected by the instruments, (iii) phase-
557 state of the bulk OA influencing the partitioning equilibrium time-scales (τ_{eq}) of the individual compounds.

558 Mass spectrometric measurement approaches provide by definition molecular formulas; however, a given formula does not
559 | correspond to an individual compound. Isaacman-VanWertz et al. (2017) showed that during the α -pinene OH oxidation
560 molecules with larger carbon atom numbers (C8 to C10) corresponded to an increased number of unique isomers for each
561 molecular formula. Differences in the functionality of these isomers may be critical for studies of their thermodynamic
562 properties. To reduce biases in this work, the different isomers seen from previous publications were included in the
563 | theoretical calculations. For the β -pinene experiment the isomers showed theoretical C* values within the estimated
564 uncertainty thus biasing to a lower extent this comparison. For formulas that corresponded to an individual compound
565 like e.g. nopinone and oxonopinone further comparison to previous publications was performed. The experimentally
566 calculated C* was in good agreement with previous studies using a GC-MS to detect particle-phase nopinone (Hohaus et al.,
567 2015;Kahnt, 2012). Since GC-MS techniques are capable of providing the exact molecular structure of nopinone this further
568 supported the identification of $(C_9H_{14}O_1)H^+$ and $(C_9H_{12}O_2)H^+$ as protonated nopinone and oxonopinone, respectively, in this
569 study.

570 The treatment of the PTR dataset to exclude ions affected by thermal and ionic dissociation was described in detail in
571 section 3.1. However, higher MW species (e.g. accretion reaction products or oligomers), of low volatility, which are not in
572 the detection range of the PTR-ToF-MS, could decompose to lower MW species during thermal breakdown (Barsanti et al.,
573 2017) (Tillmann et al., 2010). These species could be identified as a parent ion when using the parent ion identification
574 method (section 3.1) consequently inducing an overestimation of their particulate phase concentrations. This effect is not
575 constrained in the used method and could potentially and selectively decrease the volatility of certain species. To explain the
576 differences in the C* experimental vs theoretical estimations for nopinone, the ratio $\frac{G_i}{P_i}$ from equation 2 should change by a
577 factor of ~ 300 . This would suggest a particulate-phase mass concentration 300 times lower than the observed one, in order
578 to reach an agreement with the theoretical calculations. This fragmentation pathway should not only strongly affect the PTR-
579 based techniques but also the previously mentioned GC-MS systems. The decomposition pathway would be narrowed to
580 thermal dissociation during desorption, which is the only common pathway from all techniques. Finally, this thermal
581 dissociation pathway needs to result in products with the exact chemical structure of nopinone.

582 When describing SOA formation, it is generally assumed that oxidation products rapidly adopt gas-to-particle equilibrium
583 with the assumption of a homogeneously mixed condensed phase (Pankow, 1994;Odum et al., 1996). The non-ideal behavior
584 of a complex organic mixture could introduce mixing effects, changing the activity coefficients of the individual organic
585 molecules and thus their gas-to-particle equilibrium. Isotopic labeling experiments have confirmed that SOA derived from
586 different precursors will interact in a relatively ideal fashion, thus introducing minor deviations of the activity coefficient
587 | from unity (Dommen et al., 2009;Hildebrandt et al., 2011). Furthermore, Hohaus et al. (2015). Furthermore, Hohaus et al.
588 | (2015) showed that for the β -pinene ozonolysis oxidation products the theoretically estimated activity coefficient values

Formatiert: Schriftartfarbe:
Automatisch

589 | calculated by the thermodynamic group-contribution model [AIOFACAIOMFAC](#) (Zuend et al., 2011) were far from
590 | explaining the differences between theory and observations. These findings further suggest that in this work, gas-to-particle
591 | partitioning was not strongly affected by activity coefficient deviations and thus could not explain the obtained differences.
592 | On the contrary, the phase-state of the bulk OA strongly affects the partitioning equilibrium time-scales (τ_{eq}) ranging from
593 | seconds in case of liquid particles to hours or days for semi-solid or glassy particles (Shiraiwa and Seinfeld, 2012; Shiraiwa et
594 | al., 2011). Biogenic SOA particles have been found to adopt an amorphous solid-, most probably glassy-state (Virtanen et
595 | al., 2010). ~~This amorphous-~~ [The experimental conditions in this study \(on average 55 % RH\) suggest that a significant](#)
596 | [portion of the SOA can be in a semi-solid or glassy state \(Bateman et al., 2015\). This amorphous \(semi-\)solid-state may](#)
597 | influence the partitioning of semi-volatile compounds, hindering the lower volatile species to leave the particles. Biogenic
598 | OA produced in this study would be thus directly affected by high partitioning equilibrium time-scales leading to increased
599 | particulate-phase concentrations of more volatile compounds “trapped” within this glassy-state of the OA. This would imply
600 | a direct decay of their volatility thus explaining the observed lower C^* values of the 1st generation products.

601 | A comparison of the observed and calculated C^* was performed for all experiments during this campaign as shown in Figure
602 | 5. There were 11, 12 and 9 compounds observed in the limonene, terpene and trees oxidation experiments, respectively,
603 | which were described in previous publications. These compounds can be attributed to only 5, 8 and 4 different molecular
604 | formulars (m/z) suggesting an increased number of isomers found within these overlaps. The analysis yielded similar
605 | findings to those from the β -pinene experiment. The comparison between observations and theory showed relatively good
606 | agreement within the SVOC range for most of the compounds, while the C^* for compounds expected to be in the IVOC
607 | range was experimentally underestimated, i.e. the measured particle-phase concentrations were higher than those explained
608 | by the equilibrium partitioning theory. When moving from single to multiple precursor experiments e.g. from the ozonolysis
609 | of β -pinene to the ozonolysis and NO_3 oxidation of limonene, the number of isomers increased rapidly, due to the higher
610 | complexity of the investigated systems. Certain isomers showed variations up to two orders of magnitude in their estimated
611 | volatility values. On the other hand, due to increased complexity of the systems, the limitations of the mass spectrometric
612 | techniques to define the molecular structure of the compounds might introduce large biases. However, despite these
613 | uncertainties, the theoretical volatility values were still found to be in fair agreement with the observations for all systems
614 | studied, suggesting that these deviations would still be within the already existing high uncertainties associated to the
615 | theoretical calculations.

616 | There are two major effects that could be emphasized by presenting two case scenarios. In the first scenario the equilibrium
617 | partitioning theory correctly represents the studied systems. The experimental underestimation of the IVOCs (and certain
618 | SVOCs) volatility can thus only be explained by experimental uncertainties due to (i) fragmentation of higher MW
619 | compounds and oligomers to the detection range of the PTR-based techniques, and/or (ii) the existence of isomers with high
620 | volatility differences. However as mentioned before, studies which performed molecular identification of compounds (e.g.
621 | nopinone) show significantly different experimentally derived partitioning coefficient values when compared to theoretical
622 | calculations (Hohaus et al., 2015; Kahnt et al., 2012), therefore isomers could not explain this discrepancy for all cases. In
623 | the second scenario the assumption of equilibrium partitioning would be questioned due to the findings that BSOA form a
624 | glassy phase-state and thus gas-to-particle equilibrium might not be reached. This would imply that all theoretical
625 | calculations performed in this study and used in models to describe SOA formation would be developed under the wrong
626 | assumption, thus decreasing their reliability. This work provides clear evidence pointing towards these two effects but cannot
627 | provide a quantitative estimate to their individual contribution. Future studies combining the information provided by the
628 | PTR-based techniques with SOA phase-state measurements are essential. In order to bridge the gap between experimental
629 | data and theoretical volatility calculations further development of instrumentation providing structural information at a
630 | molecular level is required. Techniques like the TAG (Williams et al., 2006; Isaacman et al., 2014; Zhang et al., 2014)
631 | coupled in parallel to the PTR-based techniques could provide further insight into different isomeric structures.

633 **4 Summary**

634 We have presented the first laboratory inter-comparison of three in-situ, near real-time measurement techniques of gas-to-
635 particle partitioning with a focus on biogenic SOA formation and oxidation. These thermal desorption techniques are known
636 to be affected by thermal dissociation during desorption and ionic dissociation during ionization in the drift tube of the
637 PTRMS (Gkatzelis et al., 2017)(Gkatzelis et al., 2018). These fragmentation pathways could directly affect the gas-to-
638 particle partitioning and thus the saturation mass concentration (C^*) calculation. To reduce fragmentation biases a method to
639 identify and exclude ions affected by these decomposition pathways was developed and applied. Narrow volatility
640 distributions were observed ranging from 0 to 4 with species in the semi-volatile (SVOCs) to intermediate volatility (IVOCs)
641 regime. The limonene oxidation experiment showed a lower volatility distribution when compared to the β -pinene oxidation
642 experiment further supporting that limonene SOA are less volatile than β -pinene SOA (Lee et al., 2011). When comparing
643 C^* values obtained for species observed from all techniques, instruments showed good agreement within 1 decade, with
644 deviations explained by the different operating conditions of the PTRMS (Gkatzelis et al., 2017)(Gkatzelis et al., 2018).
645 Determined species were mapped onto the 2D-VBS framework and results showed a decrease of the C^* with increasing
646 oxidation state and increasing oxygen atom number in accordance to previous findings (Jimenez et al., 2009;Kroll, 2011).
647 These species accounted for 20-30 % of the total organic mass measured from an AMS. For species that overlapped with
648 compounds from previous publications a comparison to theoretical calculations was performed based on their molecular
649 structure. Accounting for the uncertainties of the measurements, results showed good agreement for SVOCs, while IVOCs
650 introduced higher deviations. Detailed comparison of the partitioning values of nopinone, a 1st generation product from the
651 ozonolysis of β -pinene, was performed to previous publications. Results showed agreement of the C^* within $\pm 10^{0.5}$ between
652 all experimental approaches while theory showed differences of 10^3 on the C^* estimation. These major differences are
653 discussed in terms of possible uncertainties biasing the experimental values from (1) existence of isomers within a studied
654 m/z , (2) thermal and ionic fragmentation of higher molecular weight compounds, produced by accretion and oligomerization
655 reactions, fragmenting to m/z 's detected by the instruments, (3) Non-idealities of the organic mixtures and (4) the phase-state
656 of the bulk OA affecting the partitioning equilibrium time-scales (τ_{eq}) of the individual compounds. Results point towards
657 possible interferences by thermal and ionic fragmentation as well as kinetic influences in the distribution between gas- and
658 particle-phase with diffusivity in the particle-phase and irreversible uptake. These findings further promote future work and
659 parallel measurement of the phase-state of the OA combined with compound specific volatility determination from the PTR-
660 based techniques.

661 |

← **Formatiert:** Links, Zeilenabstand:
einfach

662 **5 References**

- 663 An, W. J., Pathak, R. K., Lee, B.-H., and Pandis, S. N.: Aerosol volatility measurement using an improved thermodenuder:
664 Application to secondary organic aerosol, *J Aerosol Sci*, 38, 305-314, 10.1016/j.jaerosci.2006.12.002, 2007.
665
- 666 Barsanti, K. C., Kroll, J. H., and Thornton, J. A.: Formation of low-volatility organic compounds in the atmosphere: Recent
667 advancements and insights, *J Phys Chem Lett*, 8, 1503-1511, 10.1021/acs.jpcclett.6b02969, 2017.
668
- 669 Bateman, A. P., Gong, Z., Liu, P., Sato, B., Cirino, G., Zhang, Y., Artaxo, P., Bertram, A. K., Manzi, A. O., Rizzo, L. V.,
670 Souza, R. A. F., Zaveri, R. A., and Martin, S. T.: Sub-micrometre particulate matter is primarily in liquid form over amazon
671 rainforest, *Nat Geosci*, 9, 34, 10.1038/ngeo2599, 2015.
672
- 673 Bilde, M., Barsanti, K., Booth, M., Cappa, C. D., Donahue, N. M., Emanuelsson, E. U., McFiggans, G., Krieger, U. K.,
674 Marcolli, C., Topping, D., Ziemann, P., Barley, M., Clegg, S., Dennis-Smith, B., Hallquist, M., Hallquist, A. M., Khlystov,
675 A., Kulmala, M., Mogensen, D., Percival, C. J., Pope, F., Reid, J. P., Ribeiro da Silva, M. A., Rosenoern, T., Salo, K.,
676 Soonsin, V. P., Yli-Juuti, T., Prisle, N. L., Pagels, J., Rarey, J., Zardini, A. A., and Riipinen, I.: Saturation vapor pressures
677 and transition enthalpies of low-volatility organic molecules of atmospheric relevance: From dicarboxylic acids to complex
678 mixtures, *Chem Rev*, 115, 4115-4156, 10.1021/cr5005502, 2015.
679
- 680 Booth, A. M., Markus, T., McFiggans, G., Percival, C. J., McGillen, M. R., and Topping, D. O.: Design and construction of
681 a simple knudsen effusion mass spectrometer (kems) system for vapour pressure measurements of low volatility organics,
682 *Atmospheric Measurement Techniques*, 2, 355-361, 10.5194/amt-2-355-2009, 2009.
683
- 684 Camredon, M., Hamilton, J. F., Alam, M. S., Wyche, K. P., Carr, T., White, I. R., Monks, P. S., Rickard, A. R., and Bloss,
685 W. J.: Distribution of gaseous and particulate organic composition during dark α -pinene ozonolysis, *Atmos Chem Phys*, 10,
686 2893-2917, 2010.
687
- 688 Canagaratna, M. R., Jayne, J. T., Jimenez, J. L., Allan, J. D., Alfarra, M. R., Zhang, Q., Onasch, T. B., Drewnick, F., Coe,
689 H., Middlebrook, A., Delia, A., Williams, L. R., Trimborn, A. M., Northway, M. J., DeCarlo, P. F., Kolb, C. E., Davidovits,
690 P., and Worsnop, D. R.: Chemical and microphysical characterization of ambient aerosols with the aerodyne aerosol mass
691 spectrometer, *Mass Spectrom Rev*, 26, 185-222, 10.1002/mas.20115, 2007.
692
- 693 Canagaratna, M. R., Jimenez, J. L., Kroll, J. H., Chen, Q., Kessler, S. H., Massoli, P., Hildebrandt Ruiz, L., Fortner, E.,
694 Williams, L. R., Wilson, K. R., Surratt, J. D., Donahue, N. M., Jayne, J. T., and Worsnop, D. R.: Elemental ratio
695 measurements of organic compounds using aerosol mass spectrometry: Characterization, improved calibration, and
696 implications, *Atmos Chem Phys*, 15, 253-272, 10.5194/acp-15-253-2015, 2015.
697
- 698 Cappa, C. D., and Jimenez, J. L.: Quantitative estimates of the volatility of ambient organic aerosol, *Atmos Chem Phys*, 10,
699 5409-5424, 10.5194/acp-10-5409-2010, 2010.
700
- 701 Chen, J., and Griffin, R.: Modeling secondary organic aerosol formation from oxidation of -pinene, -pinene, and -limonene,
702 *Atmospheric Environment*, 39, 7731-7744, 10.1016/j.atmosenv.2005.05.049, 2005.
703
- 704 Clegg, S. L., Seinfeld, J. H., and Brimblecombe, P.: Thermodynamic modelling of aqueous aerosols containing electrolytes
705 and dissolved organic compounds, *J Aerosol Sci*, 32, 713-738, 2001.
706
- 707 Compernelle, S., Ceulemans, K., and Müller, J. F.: Technical note: Vapor pressure estimation methods applied to secondary
708 organic aerosol constituents from α -pinene oxidation: An intercomparison study, *Atmospheric Chemistry and Physics*, 10,
709 6271-6282, 10.5194/acp-10-6271-2010, 2010.
710
- 711 Daumit, K. E., Kessler, S. H., and Kroll, J. H.: Average chemical properties and potential formation pathways of highly
712 oxidized organic aerosol, *Faraday Discussions*, 165, 181-202, 10.1039/C3FD00045A, 2013.
713
- 714 de Gouw, J. A., Brock, C. A., Atlas, E. L., Bates, T. S., Fehsenfeld, F. C., Goldan, P. D., Holloway, J. S., Kuster, W. C.,
715 Lerner, B. M., Matthew, B. M., Middlebrook, A. M., Onasch, T. B., Peltier, R. E., Quinn, P. K., Senff, C. J., Stohl, A.,
716 Sullivan, A. P., Trainer, M., Warneke, C., Weber, R. J., and Williams, E. J.: Sources of particulate matter in the northeastern
717 united states in summer: 1. Direct emissions and secondary formation of organic matter in urban plumes, *J Geophys Res*,
718 113, 10.1029/2007jd009243, 2008.
719
- 720 DeCarlo, P. F., Kimmel, J. R., Trimborn, A., Northway, M. J., Jayne, J. T., Aiken, A. C., Gonin, M., Fuhrer, K., Horvath, T.,
721 Docherty, K. S., Worsnop, D. R., and Jimenez, J. L.: Field-deployable, high-resolution, time-of-flight aerosol mass
722 spectrometer, *Anal Chem*, 78, 8281-8289, 10.1021/ac061249n, 2006.
723

724 Dommen, J., Hellén, H., Saurer, M., Jaeggi, M., Siegwolf, R., Metzger, A., Duplissy, J., Fierz, M., and Baltensperger, U.:
725 Determination of the aerosol yield of isoprene in the presence of an organic seed with carbon isotope analysis, *Environ Sci*
726 *Technol*, 43, 6697-6702, 10.1021/es9006959, 2009.

727

728 Donahue, N. M., Robinson, A. L., Stanier, C. O., and Pandis, S. N.: Coupled partitioning, dilution, and chemical aging of
729 semivolatile organics, *Environ Sci Technol*, 40, 2635-2643, 10.1021/es052297c, 2006.

730

731 Donahue, N. M., Epstein, S. A., Pandis, S. N., and Robinson, A. L.: A two-dimensional volatility basis set: 1. Organic-
732 aerosol mixing thermodynamics, *Atmos Chem Phys*, 11, 3303-3318, 10.5194/acp-11-3303-2011, 2011.

733

734 Donahue, N. M., Kroll, J. H., Pandis, S. N., and Robinson, A. L.: A two-dimensional volatility basis set – part 2: Diagnostics
735 of organic-aerosol evolution, *Atmospheric Chemistry and Physics*, 12, 615-634, 10.5194/acp-12-615-2012, 2012.

736

737 Donahue, N. M., Chuang, W., Epstein, S. A., Kroll, J. H., Worsnop, D. R., Robinson, A. L., Adams, P. J., and Pandis, S. N.:
738 Why do organic aerosols exist? Understanding aerosol lifetimes using the two-dimensional volatility basis set,
739 *Environmental Chemistry*, 10, 151, 10.1071/en13022, 2013.

740

741 Donahue, N. M., Robinson, A. L., Trump, E. R., Riipinen, I., and Kroll, J. H.: Volatility and aging of atmospheric organic
742 aerosol, *Top Curr Chem*, 339, 97-143, 10.1007/128_2012_355, 2014.

743

744 Duncianu, M., David, M., Kartigeyane, S., Cirtog, M., Doussin, J. F., and Picquet-Varrault, B.: Measurement of alkyl and
745 multifunctional organic nitrates by proton-transfer-reaction mass spectrometry, *Atmos Meas Tech*, 10, 1445-1463,
746 10.5194/amt-10-1445-2017, 2017.

747

748 Ehn, M., Thornton, J. A., Kleist, E., Sipila, M., Junninen, H., Pullinen, I., Springer, M., Rubach, F., Tillmann, R., Lee, B.,
749 Lopez-Hilfiker, F., Andres, S., Acir, I. H., Rissanen, M., Jokinen, T., Schobesberger, S., Kangasluoma, J., Kontkanen, J.,
750 Nieminen, T., Kurten, T., Nielsen, L. B., Jorgensen, S., Kjaergaard, H. G., Canagaratna, M., Maso, M. D., Berndt, T., Petaja,
751 T., Wahner, A., Kerminen, V. M., Kulmala, M., Worsnop, D. R., Wildt, J., and Mentel, T. F.: A large source of low-
752 volatility secondary organic aerosol, *Nature*, 506, 476-479, 10.1038/nature13032, 2014.

753

754 Eichler, P., Müller, M., D'Anna, B., and Wisthaler, A.: A novel inlet system for online chemical analysis of semi-volatile
755 submicron particulate matter, *Atmos Meas Tech*, 8, 1353-1360, DOI 10.5194/amt-8-1353-2015, 2015.

756

757 Eichler, P., Müller, M., Rohmann, C., Stengel, B., Orasche, J., Zimmermann, R., and Wisthaler, A.: Lubricating oil as a
758 major constituent of ship exhaust particles, *Environmental Science & Technology Letters*, 4, 54-58,
759 10.1021/acs.estlett.6b00488, 2017.

760

761 Epstein, S. A., Riipinen, I., and Donahue, N. M.: A semiempirical correlation between enthalpy of vaporization and
762 saturation concentration for organic aerosol, *Environmental science & technology*, 44, 743-748, 10.1021/es902497z, 2010.

763

764 Faulhaber, A. E., Thomas, B. M., Jimenez, J. L., Jayne, J. T., Worsnop, D. R., and Ziemann, P. J.: Characterization of a
765 thermodesorption-particle beam mass spectrometer system for the study of organic aerosol volatility and composition, *Atmos*
766 *Meas Tech*, 2, 15-31, 10.5194/amt-2-15-2009, 2009.

767

768 Fredenslund, A., Jones, R. L., and Prausnitz, J. M.: Group-contribution estimation of activity coefficients in nonideal liquid
769 mixtures, *AIChE J*, 21, 1086-1099, 1975.

770

771 Gkatzelis, G. I., Papanastasiou, D. K., Florou, K., Kaltsonoudis, C., Louvaris, E., and Pandis, S. N.: Measurement of
772 nonvolatile particle number size distribution, *Atmos Meas Tech*, 9, 103-114, 10.5194/amt-9-103-2016, 2016.

773

774 Gkatzelis, G. I., Tillmann, R., Hohaus, T., Müller, M., Eichler, P., Xu, K.-M., Schlag, P., Schmitt, S. H., Wegener, R.,
775 Kaminski, M., Holzinger, R., Wisthaler, A., and Kiendler-Scharr, A.: Comparison of three aerosol chemical characterization
776 techniques utilizing ptr-tof-ms: A study on freshly formed and aged biogenic soa, *Atmospheric Measurement Techniques*
777 *Discussions*, 1-31, 10.5194/amt-2017-288, 2017.

778

779 Gkatzelis, G. I., Tillmann, R., Hohaus, T., Müller, M., Eichler, P., Xu, K. M., Schlag, P., Schmitt, S. H., Wegener, R.,
780 Kaminski, M., Holzinger, R., Wisthaler, A., and Kiendler-Scharr, A.: Comparison of three aerosol chemical characterization
781 techniques utilizing ptr-tof-ms: A study on freshly formed and aged biogenic soa, *Atmos. Meas. Tech.*, 11, 1481-1500,
782 10.5194/amt-11-1481-2018, 2018.

783

784 Goldstein, A. H., Worton, D. R., Williams, B. J., Hering, S. V., Kreisberg, N. M., Panić, O., and Górecki, T.: Thermal
785 desorption comprehensive two-dimensional gas chromatography for in-situ measurements of organic aerosols, *J Chromatogr*
786 *A*, 1186, 340-347, <https://doi.org/10.1016/j.chroma.2007.09.094>, 2008.

787

788 Hallquist, M., Wenger, J. C., Baltensperger, U., Rudich, Y., Simpson, D., Claeys, M., Dommen, J., Donahue, N. M., George,
789 C., Goldstein, A. H., Hamilton, J. F., Herrmann, H., Hoffmann, T., Iinuma, Y., Jang, M., Jenkin, M. E., Jimenez, J. L.,
790 Kiendler-Scharr, A., Maenhaut, W., McFiggans, G., Mentel, T. F., Monod, A., Prévôt, A. S. H., Seinfeld, J. H., Surratt, J. D.,
791 Szmigielski, R., and Wildt, J.: The formation, properties and impact of secondary organic aerosol: Current and emerging
792 issues, *Atmos Chem Phys*, 9, 5155-5236, 10.5194/acp-9-5155-2009, 2009.

793
794 Hildebrandt, L., Henry, K. M., Kroll, J. H., Worsnop, D. R., Pandis, S. N., and Donahue, N. M.: Evaluating the mixing of
795 organic aerosol components using high-resolution aerosol mass spectrometry, *Environ Sci Technol*, 45, 6329-6335,
796 10.1021/es200825g, 2011.

797
798 Hohaus, T., Trimborn, D., Kiendler-Scharr, A., Gensch, I., Laumer, W., Kammer, B., Andres, S., Boudries, H., Smith, K. A.,
799 Worsnop, D. R., and Jayne, J. T.: A new aerosol collector for quasi on-line analysis of particulate organic matter: The
800 aerosol collection module (acm) and first applications with a gc/ms-fid, *Atmos Meas Tech*, 3, 1423-1436, DOI 10.5194/amt-
801 3-1423-2010, 2010.

802
803 Hohaus, T., Gensch, I., Kimmel, J. R., Worsnop, D. R., and Kiendler-Scharr, A.: Experimental determination of the
804 partitioning coefficient of β -pinene oxidation products in soas, *Physical Chemistry Chemical Physics*, 17, 14796-14804,
805 10.1039/C5CP01608H, 2015.

806
807 Hohaus, T., Kuhn, U., Andres, S., Kaminski, M., Rohrer, F., Tillmann, R., Wahner, A., Wegener, R., Yu, Z., and Kiendler-
808 Scharr, A.: A new plant chamber facility, plus, coupled to the atmosphere simulation chamber saphir, *Atmos Meas Tech*, 9,
809 1247-1259, 10.5194/amt-9-1247-2016, 2016.

810
811 Holzinger, R., Williams, J., Herrmann, F., Lelieveld, J., Donahue, N. M., and Rockmann, T.: Aerosol analysis using a
812 thermal-desorption proton-transfer-reaction mass spectrometer (td-ptr-ms): A new approach to study processing of organic
813 aerosols, *Atmos Chem Phys*, 10, 2257-2267, 2010.

814
815 Huffman, J. A., Ziemann, P. J., Jayne, J. T., Worsnop, D. R., and Jimenez, J. L.: Development and characterization of a fast-
816 stepping/scanning thermodenuder for chemically-resolved aerosol volatility measurements, *Aerosol Sci Tech*, 42, 395-407,
817 10.1080/02786820802104981, 2008.

818
819 Isaacman-VanWertz, G., Yee, L. D., Kreisberg, N. M., Wernis, R., Moss, J. A., Hering, S. V., de Sa, S. S., Martin, S. T.,
820 Alexander, M. L., Palm, B. B., Hu, W., Campuzano-Jost, P., Day, D. A., Jimenez, J. L., Riva, M., Surratt, J. D., Viegas, J.,
821 Manzi, A., Edgerton, E., Baumann, K., Souza, R., Artaxo, P., and Goldstein, A. H.: Ambient gas-particle partitioning of
822 tracers for biogenic oxidation, *Environmental science & technology*, 10.1021/acs.est.6b01674, 2016.

823
824 Isaacman-VanWertz, G., Massoli, P., O'Brien, R. E., Nowak, J. B., Canagaratna, M. R., Jayne, J. T., Worsnop, D. R., Su, L.,
825 Knopf, D. A., Misztal, P. K., Arata, C., Goldstein, A. H., and Kroll, J. H.: Using advanced mass spectrometry techniques to
826 fully characterize atmospheric organic carbon: Current capabilities and remaining gaps, *Faraday Discussions*,
827 10.1039/C7FD00021A, 2017.

828
829 Isaacman, G., Worton, D. R., Kreisberg, N. M., Hennigan, C. J., Teng, A. P., Hering, S. V., Robinson, A. L., Donahue, N.
830 M., and Goldstein, A. H.: Understanding evolution of product composition and volatility distribution through in-situ gc x gc
831 analysis: A case study of longifolene ozonolysis, *Atmospheric Chemistry and Physics*, 11, 5335-5346, 10.5194/acp-11-5335-
832 2011, 2011.

833
834 Isaacman, G., Kreisberg, N. M., Yee, L. D., Worton, D. R., Chan, A. W. H., Moss, J. A., Hering, S. V., and Goldstein, A. H.:
835 Online derivatization for hourly measurements of gas- and particle-phase semi-volatile oxygenated organic compounds by
836 thermal desorption aerosol gas chromatography (sv-tag), *Atmos Meas Tech*, 7, 4417-4429, DOI 10.5194/amt-7-4417-2014,
837 2014.

838
839 Jang, M., and Kamens, R. M.: Atmospheric secondary aerosol formation by heterogeneous reactions of aldehydes in the
840 presence of a sulfuric acid aerosol catalyst, *Environ Sci Technol*, 35, 4758-4766, 10.1021/es010790s, 2001.

841
842 Jaoui, M., Corse, E., Kleindienst, T. E., Offenberg, J. H., Lewandowski, M., and Edney, E. O.: Analysis of secondary
843 organic aerosol compounds from the photooxidation of d-limonene in the presence of nox and their detection in ambient
844 pm_{2.5}, *Environmental Science & Technology*, 40, 3819-3828, 10.1021/es052566z, 2006.

845
846 Jenkin, M. E.: Modelling the formation and composition of secondary organic aerosol from α - and β -pinene ozonolysis
847 using mcm v3 *Atmospheric Chemistry and Physics*, 4, 1741-1757, 2004.

848
849 Jimenez, J. L., Canagaratna, M. R., Donahue, N. M., Prevot, A. S. H., Zhang, Q., Kroll, J. H., DeCarlo, P. F., Allan, J. D.,
850 Coe, H., Ng, N. L., Aiken, A. C., Docherty, K. S., Ulbrich, I. M., Grieshop, A. P., Robinson, A. L., Duplissy, J., Smith, J. D.,
851 Wilson, K. R., Lanz, V. A., Hueglin, C., Sun, Y. L., Tian, J., Laaksonen, A., Raatikainen, T., Rautiainen, J., Vaattovaara, P.,

852 Ehn, M., Kulmala, M., Tomlinson, J. M., Collins, D. R., Cubison, M. J., Dunlea, J., Huffman, J. A., Onasch, T. B., Alfarra,
853 M. R., Williams, P. I., Bower, K., Kondo, Y., Schneider, J., Drewnick, F., Borrmann, S., Weimer, S., Demerjian, K.,
854 Salcedo, D., Cottrell, L., Griffin, R., Takami, A., Miyoshi, T., Hatakeyama, S., Shimojo, A., Sun, J. Y., Zhang, Y. M.,
855 Dzepina, K., Kimmel, J. R., Sueper, D., Jayne, J. T., Herndon, S. C., Trimborn, A. M., Williams, L. R., Wood, E. C.,
856 Middlebrook, A. M., Kolb, C. E., Baltensperger, U., and Worsnop, D. R.: Evolution of organic aerosols in the atmosphere,
857 Science, 326, 10.1126/science.1180353, 2009.
858
859 Joback, K. G., and Reid, R. C.: Estimation of pure-component properties from group contributions, Chem Eng Commun, 57,
860 233-243, 10.1080/00986448708960487, 1987.
861
862 Kahnt, A.: Semivolatile compounds from atmospheric monoterpene oxidation PhD, Fakultät für Chemie und Mineralogie,
863 Universität Leipzig, Leipzig, Germany, 205 pp., 2012.
864
865 Karnezi, E., Riipinen, I., and Pandis, S. N.: Measuring the atmospheric organic aerosol volatility distribution: A theoretical
866 analysis, Atmospheric Measurement Techniques, 7, 2953-2965, 10.5194/amt-7-2953-2014, 2014.
867
868 Krechmer, J. E., Coggon, M. M., Massoli, P., Nguyen, T. B., Crouse, J. D., Hu, W., Day, D. A., Tyndall, G. S., Henze, D.
869 K., Rivera-Rios, J. C., Nowak, J. B., Kimmel, J. R., Mauldin, R. L., 3rd, Stark, H., Jayne, J. T., Sipila, M., Junninen, H.,
870 Clair, J. M., Zhang, X., Feiner, P. A., Zhang, L., Miller, D. O., Brune, W. H., Keutsch, F. N., Wennberg, P. O., Seinfeld, J.
871 H., Worsnop, D. R., Jimenez, J. L., and Canagaratna, M. R.: Formation of low volatility organic compounds and secondary
872 organic aerosol from isoprene hydroxyhydroperoxide low-no oxidation, Environ Sci Technol, 49, 10330-10339,
873 10.1021/acs.est.5b02031, 2015.
874
875 Kreisberg, N. M., Hering, S. V., Williams, B. J., Worton, D. R., and Goldstein, A. H.: Quantification of hourly speciated
876 organic compounds in atmospheric aerosols, measured by an in-situ thermal desorption aerosol gas chromatograph (tag),
877 Aerosol Sci Tech, 43, 38-52, 10.1080/02786820802459583, 2009.
878
879 Kroll, J. H.: Carbon oxidation state as a metric for describing the chemistry of atmospheric organic aerosol, Nat Chem, 3,
880 10.1038/nchem.948, 2011.
881
882 Kundu, S., Fisseha, R., Putman, A. L., Rahn, T. A., and Mazzoleni, L. R.: High molecular weight soa formation during
883 limonene ozonolysis: Insights from ultrahigh-resolution fit-icr mass spectrometry characterization, Atmospheric Chemistry
884 and Physics, 12, 5523-5536, 10.5194/acp-12-5523-2012, 2012.
885
886 Lee, B.-H., Pierce, J. R., Engelhart, G. J., and Pandis, S. N.: Volatility of secondary organic aerosol from the ozonolysis of
887 monoterpenes, Atmospheric Environment, 45, 2443-2452, 10.1016/j.atmosenv.2011.02.004, 2011.
888
889 Leungsakul, S., Jaoui, M., and Kamens, R. M.: Kinetic mechanism for predicting secondary organic aerosol formation from
890 the reaction of d-limonene with ozone, Environmental Science & Technology, 39, 9583-9594, 10.1021/es0492687, 2005a.
891
892 Leungsakul, S., Jeffries, H. E., and Kamens, R. M.: A kinetic mechanism for predicting secondary aerosol formation from
893 the reactions of d-limonene in the presence of oxides of nitrogen and natural sunlight, Atmospheric Environment, 39, 7063-
894 7082, 10.1016/j.atmosenv.2005.08.024, 2005b.
895
896 Li, Y., Pöschl, U., and Shiraiwa, M.: Molecular corridors and parameterizations of volatility in the chemical evolution of
897 organic aerosols, Atmos. Chem. Phys., 16, 3327-3344, 10.5194/acp-16-3327-2016, 2016.
898
899 Lopez-Hilfiker, F. D., Mohr, C., Ehn, M., Rubach, F., Kleist, E., Wildt, J., Mentel, T. F., Lutz, A., Hallquist, M., Worsnop,
900 D., and Thornton, J. A.: A novel method for online analysis of gas and particle composition: Description and evaluation of a
901 filter inlet for gases and aerosols (figaero), Atmos Meas Tech, 7, 983-1001, DOI 10.5194/amt-7-983-2014, 2014.
902
903 Lopez-Hilfiker, F. D., Mohr, C., Ehn, M., Rubach, F., Kleist, E., Wildt, J., Mentel, T. F., Carrasquillo, A. J., Daumit, K. E.,
904 Hunter, J. F., Kroll, J. H., Worsnop, D. R., and Thornton, J. A.: Phase partitioning and volatility of secondary organic aerosol
905 components formed from α -pinene ozonolysis and oh oxidation: The importance of accretion products and other low
906 volatility compounds, Atmos Chem Phys, 15, 7765-7776, 10.5194/acp-15-7765-2015, 2015.
907
908 Lopez-Hilfiker, F. D., Mohr, C., D'Ambro, E. L., Lutz, A., Riedel, T. P., Gaston, C. J., Iyer, S., Zhang, Z., Gold, A., Surratt,
909 J. D., Lee, B. H., Kurten, T., Hu, W. W., Jimenez, J., Hallquist, M., and Thornton, J. A.: Molecular composition and
910 volatility of organic aerosol in the southeastern u.s.: Implications for iepox derived soa, Environ Sci Technol, 50, 2200-
911 2209, 10.1021/acs.est.5b04769, 2016.
912
913 Louvaris, E. E., Florou, K., Karnezi, E., Papanastasiou, D. K., Gkatzelis, G. I., and Pandis, S. N.: Volatility of source
914 apportioned wintertime organic aerosol in the city of athens, Atmos Environ, 158, 138-147,
915 10.1016/j.atmosenv.2017.03.042, 2017.

916
917 Mackay, D., Bobra, A., Chan, D. W., and Shiu, W. Y.: Vapor-pressure correlations for low-volatility environmental
918 chemicals, *Environ Sci Technol*, 16, 645-649, 10.1021/es00104a004, 1982.
919
920 Martinez, R. E., Williams, B. J., Zhang, Y., Hagan, D., Walker, M., Kreisberg, N. M., Hering, S. V., Hohaus, T., Jayne, J. T.,
921 and Worsnop, D. R.: Development of a volatility and polarity separator (vaps) for volatility- and polarity-resolved organic
922 aerosol measurement, *Aerosol Sci Tech*, 50, 255-271, 10.1080/02786826.2016.1147645, 2016.
923
924 McFiggans, G., Topping, D. O., and Barley, M. H.: The sensitivity of secondary organic aerosol component partitioning to
925 the predictions of component properties – part 1: A systematic evaluation of some available estimation techniques,
926 *Atmospheric Chemistry and Physics*, 10, 10255-10272, 10.5194/acp-10-10255-2010, 2010.
927
928 Mitchem, L., and Reid, J. P.: Optical manipulation and characterisation of aerosol particles using a single-beam gradient
929 force optical trap, *Chem Soc Rev*, 37, 756-769, 10.1039/b609713h, 2008.
930
931 Murphy, B. N., Donahue, N. M., Fountoukis, C., Dall'Osto, M., O'Dowd, C., Kiendler-Scharr, A., and Pandis, S. N.:
932 Functionalization and fragmentation during ambient organic aerosol aging: Application of the 2-d volatility basis set to field
933 studies, *Atmospheric Chemistry and Physics*, 12, 10797-10816, 10.5194/acp-12-10797-2012, 2012.
934
935 Myrdal, P. B., and Yalkowsky, S. H.: Estimating pure component vapor pressures of complex organic molecules, *Ind Eng*
936 *Chem Res*, 36, 2494-2499, 10.1021/ie950242l, 1997.
937
938 Nannoolal, Y., Rarey, J., and Ramjugernath, D.: Estimation of pure component properties. Part 3. Estimation of the vapor
939 pressure of non-electrolyte organic compounds via group contributions and group interaction, *Fluid Phase Equilib*, 269, 117-
940 133, 10.1016/j.fluid.2008.04.020, 2008.
941
942 Odum, J. R., Hoffmann, T., Bowman, F., Collins, D., Flagan, R. C., and Seinfeld, J. H.: Gas/particle partitioning and
943 secondary organic aerosol yields, *Environmental science & technology*, 30, 2580-2585, 10.1021/es950943+, 1996.
944
945 Pankow, J. F.: An absorption model of gas/particle partitioning of organic compounds in the atmosphere, *Atmospheric*
946 *Environment*, 28, 185-188, 1994.
947
948 Pankow, J. F., and Asher, W. E.: Simpol.1: A simple group contribution method for predicting vapor pressures and
949 enthalpies of vaporization of multifunctional organic compounds, *Atmos Chem Phys*, 8, 2773-2796, 10.5194/acp-8-2773-
950 2008, 2008.
951
952 Pankow, J. F., and Barsanti, K. C.: The carbon number-polarity grid: A means to manage the complexity of the mix of
953 organic compounds when modeling atmospheric organic particulate matter, *Atmospheric Environment*, 43, 2829-2835,
954 10.1016/j.atmosenv.2008.12.050, 2009.
955
956 Pope, F. D., Dennis-Smith, B. J., Griffiths, P. T., Clegg, S. L., and Cox, R. A.: Studies of single aerosol particles
957 containing malonic acid, glutaric acid, and their mixtures with sodium chloride. I. Hygroscopic growth, *J Phys Chem-US*,
958 114, 5335-5341, 2010.
959
960 Praplan, A. P., Schobesberger, S., Bianchi, F., Rissanen, M. P., Ehn, M., Jokinen, T., Junninen, H., Adamov, A., Amorim,
961 A., Dommen, J., Duplissy, J., Hakala, J., Hansel, A., Heinritzi, M., Kangasluoma, J., Kirkby, J., Krapf, M., Kürten, A.,
962 Lehtipalo, K., Riccobono, F., Rondo, L., Sarnela, N., Simon, M., Tomé, A., Tröstl, J., Winkler, P. M., Williamson, C., Ye,
963 P., Curtius, J., Baltensperger, U., Donahue, N. M., Kulmala, M., and Worsnop, D. R.: Elemental composition and clustering
964 of α -pinene oxidation products for different oxidation conditions, *Atmospheric Chemistry and Physics Discussions*, 14,
965 30799-30833, 10.5194/acpd-14-30799-2014, 2014.
966
967 Prisle, N. L., Engelhart, G. J., Bilde, M., and Donahue, N. M.: Humidity influence on gas-particle phase partitioning of α -
968 pinene + α -secondary organic aerosol, *Geophysical Research Letters*, 37, n/a-n/a, 10.1029/2009gl041402, 2010.
969
970 Riipinen, I., Pierce, J. R., Donahue, N. M., and Pandis, S. N.: Equilibration time scales of organic aerosol inside
971 thermodenuders: Evaporation kinetics versus thermodynamics, *Atmospheric Environment*, 44, 597-607,
972 10.1016/j.atmosenv.2009.11.022, 2010.
973
974 Rohrer, F., Bohn, B., Brauers, T., Brüning, D., Johnen, F. J., Wahner, A., and Kleffmann, J.: Characterisation of the
975 photolytic hono-source in the atmosphere simulation chamber saphir, *Atmospheric Chemistry and Physics*, 5, 2189-2201,
976 10.5194/acp-5-2189-2005, 2005.
977
978 Shiraiwa, M., Ammann, M., Koop, T., and Pöschl, U.: Gas uptake and chemical aging of semisolid organic aerosol particles,
979 *PNAS*, 108, 11003-11008, 10.1073/pnas.1103045108, 2011.

980
981 Shiraiwa, M., and Seinfeld, J. H.: Equilibration timescale of atmospheric secondary organic aerosol partitioning,
982 *Geophysical Research Letters*, 39, n/a-n/a, 10.1029/2012gl054008, 2012.
983
984 Stark, H., Yatavelli, R. L. N., Thompson, S. L., Kang, H., Krechmer, J. E., Kimmel, J. R., Palm, B. B., Hu, W., Hayes, P. L.,
985 Day, D. A., Campuzano-Jost, P., Canagaratna, M. R., Jayne, J. T., Worsnop, D. R., and Jimenez, J. L.: Impact of thermal
986 decomposition on thermal desorption instruments: Advantage of thermogram analysis for quantifying volatility distributions
987 of organic species, *Environ Sci Technol*, 10.1021/acs.est.7b00160, 2017.
988
989 Stein, S. E., and Brown, R. L.: Estimation of normal boiling points from group contributions, *J Chem Inf Comp Sci*, 34, 581-
990 587, 1994.
991
992 Steitz, B.: Experimental determination of the partitioning coefficient of nopinone as a marker substance in organic aerosol,
993 PhD, Institute of Energy and Climate: Troposphere (IEK-8), Wuppertal University, Forschungszentrum Jülich GmbH, 2010.
994
995 Thompson, S. L., Yatavelli, R. L. N., Stark, H., Kimmel, J. R., Krechmer, J. E., Day, D. A., Hu, W., Isaacman-VanWertz,
996 G., Yee, L., Goldstein, A. H., Khan, M. A. H., Holzinger, R., Kreisberg, N., Lopez-Hilfiker, F. D., Mohr, C., Thornton, J. A.,
997 Jayne, J. T., Canagaratna, M., Worsnop, D. R., and Jimenez, J. L.: Field intercomparison of the gas/particle partitioning of
998 oxygenated organics during the southern oxidant and aerosol study (soas) in 2013, *Aerosol Sci Tech*, 51, 30-56,
999 10.1080/02786826.2016.1254719, 2017.
1000
1001 Tobias, H. J., and Ziemann, P. J.: Compound identification in organic aerosols using temperature-programmed thermal
1002 desorption particle beam mass spectrometry, *Anal Chem*, 71, 3428-3435, 10.1021/ac990056f, 1999.
1003
1004 Tobias, H. J., and Ziemann, P. J.: Kinetics of the gas-phase reactions of alcohols, aldehydes, carboxylic acids, and water with
1005 the c13 stabilized criegee intermediate formed from ozonolysis of 1-tetradecene, *The Journal of Physical Chemistry A*, 105,
1006 6129-6135, 10.1021/jp004631r, 2001.
1007
1008 Virtanen, A., Joutsensaari, J., Koop, T., Kannosto, J., Yli-Pirila, P., Leskinen, J., Makela, J. M., Holopainen, J. K., Poschl,
1009 U., Kulmala, M., Worsnop, D. R., and Laaksonen, A.: An amorphous solid state of biogenic secondary organic aerosol
1010 particles, *Nature*, 467, 824-827, 10.1038/nature09455, 2010.
1011
1012 Volkamer, R., Jimenez, J. L., San Martini, F., Dzepina, K., Zhang, Q., Salcedo, D., Molina, L. T., Worsnop, D. R., and
1013 Molina, M. J.: Secondary organic aerosol formation from anthropogenic air pollution: Rapid and higher than expected,
1014 *Geophys Res Lett*, 33, 10.1029/2006gl026899, 2006.
1015
1016 Williams, B. J., Goldstein, A. H., Kreisberg, N. M., and Hering, S. V.: An in-situ instrument for speciated organic
1017 composition of atmospheric aerosols: Thermal desorption aerosol gas chromatograph/mass spectrometer (tag-ams), *Aerosol Sci Tech*, 40,
1018 627-638, 10.1080/02786820600754631, 2006.
1019
1020 Williams, B. J., Jayne, J. T., Lambe, A. T., Hohaus, T., Kimmel, J. R., Sueper, D., Brooks, W., Williams, L. R., Trimborn,
1021 A. M., Martinez, R. E., Hayes, P. L., Jimenez, J. L., Kreisberg, N. M., Hering, S. V., Worton, D. R., Goldstein, A. H., and
1022 Worsnop, D. R.: The first combined thermal desorption aerosol gas chromatograph— aerosol mass spectrometer (tag-ams),
1023 *Aerosol Sci Tech*, 48, 358-370, 10.1080/02786826.2013.875114, 2014.
1024
1025 Williams, B. J., Zhang, Y., Zuo, X., Martinez, R. E., Walker, M. J., Kreisberg, N. M., Goldstein, A. H., Docherty, K. S., and
1026 Jimenez, J. L.: Organic and inorganic decomposition products from the thermal desorption of atmospheric particles, *Atmos.*
1027 *Meas. Tech.*, 9, 1569-1586, 10.5194/amt-9-1569-2016, 2016.
1028
1029 Yatavelli, R. L. N., Stark, H., Thompson, S. L., Kimmel, J. R., Cubison, M. J., Day, D. A., Campuzano-Jost, P., Palm, B. B.,
1030 Hodzic, A., Thornton, J. A., Jayne, J. T., Worsnop, D. R., and Jimenez, J. L.: Semicontinuous measurements of gas-particle
1031 partitioning of organic acids in a ponderosa pine forest using a movi-hrtof-cims, *Atmos Chem Phys*, 14, 1527-1546, DOI
1032 10.5194/acp-14-1527-2014, 2014.
1033
1034 Yu, J., Cocker, D. R., Griffin, R. J., Flagan, R. C., and Seinfeld, J. H.: Gas-phase ozone oxidation of monoterpenes: Gaseous
1035 and particulate products, *Journal of Atmospheric Chemistry*, 34, 207-258, 10.1023/a:1006254930583, 1999.
1036
1037 Zhang, Y. P., Williams, B. J., Goldstein, A. H., Docherty, K., Ulbrich, I. M., and Jimenez, J. L.: A technique for rapid gas
1038 chromatography analysis applied to ambient organic aerosol measurements from the thermal desorption aerosol gas
1039 chromatograph (tag), *Aerosol Sci Tech*, 48, 1166-1182, Doi 10.1080/02786826.2014.967832, 2014.
1040
1041 Zhao, Y., Kreisberg, N. M., Worton, D. R., Isaacman, G., Weber, R. J., Liu, S., Day, D. A., Russell, L. M., Markovic, M. Z.,
1042 VandenBoer, T. C., Murphy, J. G., Hering, S. V., and Goldstein, A. H.: Insights into secondary organic aerosol formation

1043 mechanisms from measured gas/particle partitioning of specific organic tracer compounds, *Environ Sci Technol*, 47, 3781-
1044 3787, 10.1021/es304587x, 2013a.

1045
1046 Zhao, Y., Kreisberg, N. M., Worton, D. R., Teng, A. P., Hering, S. V., and Goldstein, A. H.: Development of an in
1047 situ thermal desorption gas chromatography instrument for quantifying atmospheric semi-volatile organic compounds,
1048 *Aerosol Sci Tech*, 47, 258-266, 10.1080/02786826.2012.747673, 2013b.

1049
1050 Zuend, A., Marcolli, C., Booth, A. M., Lienhard, D. M., Soonsin, V., Krieger, U. K., Topping, D. O., McFiggans, G., Peter,
1051 T., and Seinfeld, J. H.: New and extended parameterization of the thermodynamic model aiomfac: Calculation of activity
1052 coefficients for organic-inorganic mixtures containing carboxyl, hydroxyl, carbonyl, ether, ester, alkenyl, alkyl, and aromatic
1053 functional groups, *Atmos Chem Phys*, 11, 9155-9206, DOI 10.5194/acp-11-9155-2011, 2011.

1054
1055

1056

1057

1058

1059

1060

1061

1062

1063

1064

1065

1066

1067

1068

1069

1070

1071

1072

1073

1074

1075

1076

1077

1078

1079

1080

1081

1082

1083

1084

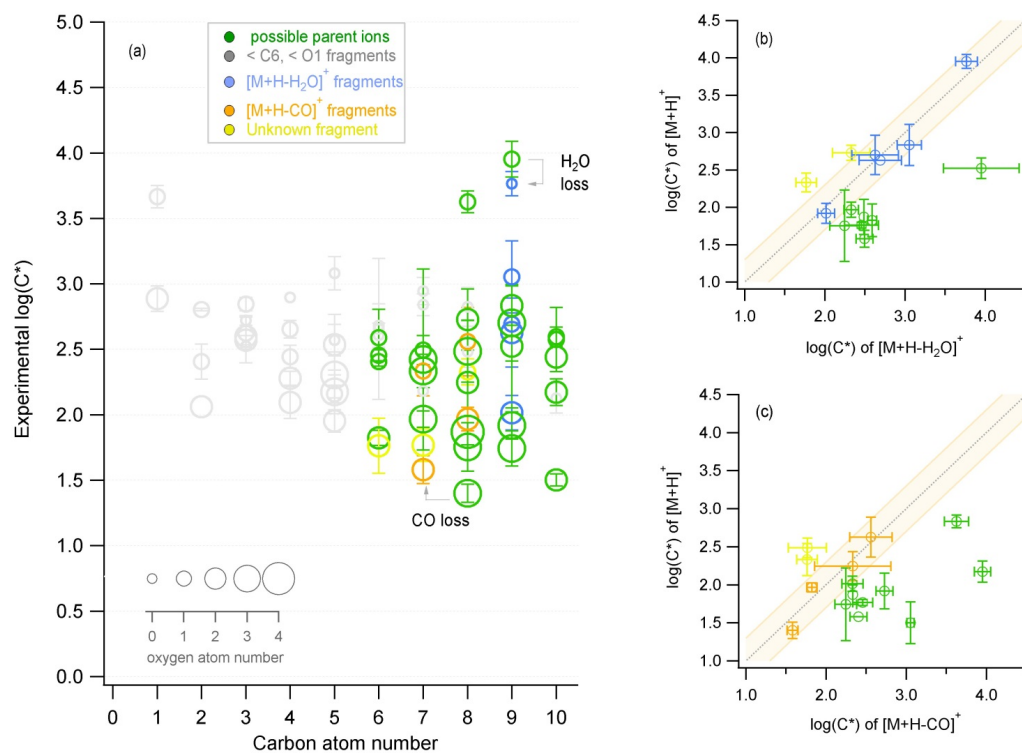
1085

1086

1087 **Table 1: Experimental conditions during each ozonolysis experiment. Two VOC injection periods were performed for the tree**
 1088 **emissions experiment.**

Experiment	Ozone (ppb vppb <u>v</u>)	Monoterpenes (ppb vppbv)	Duration (h)	Maximum SOA formed ($\mu\text{g}/\text{m}^3$)	Chamber temperature ($^{\circ}\text{C}$)	SOA aging Conditions
β-Pinene	700	120	34	130	20 ± 4	Photochemical oxidation for 10 h
Limonene	150	25	17	50	17 ± 4	Continuous NO_3 oxidation for 8 h
β-Pinene/Limonene mixture	300	60/12	26	60	19 ± 5	Photochemical oxidation for 4 h
Tree emissions 1 st inj. / 2 nd inj.	300	65/10	30	80	30 ± 5	Photochemical oxidation for 6 h

1089
 1090
 1091
 1092
 1093
 1094
 1095



1097

1098 **Figure 1: Characteristic example of fragment identification method from the β -pinene ozonolysis experiment for the ACM where**
 1099 **(a) is the experimental saturation concentration (y-axis) for all identified compounds with different carbon (x-axis) and oxygen**
 1100 **atom number (size of markers). Different colors indicate whether the compound represents a possible parent ion (green), a**
 1101 **fragment with carbon and oxygen atom number lower than 6 and 1 respectively (grey), or a fragment originating from the loss of**
 1102 **water (blue) or CO (orange). This attribution results from Figure (b) and (c) which show the correlation of the saturation**
 1103 **concentration of identified $[M+H]^+$ ions to compounds with the same chemical formula subtracting water $[M+H-H_2O]^+$ or CO**
 1104 **$[M+H-CO]^+$. If the correlation is close to the 1:1 line then the $[M+H-H_2O]^+$ or $[M+H-CO]^+$ compound is identified as a fragment**
 1105 **and is given the respective color (blue or orange). If the $[M+H-H_2O]^+$ or $[M+H-CO]^+$ compound shows a higher volatility it**
 1106 **is considered as a possible parent ion (green). The orange background indicates the ± 0.25 change of $\log(C^*)$. Error bars correspond**
 1107 **to the error of the average ($\pm 1\sigma$).**

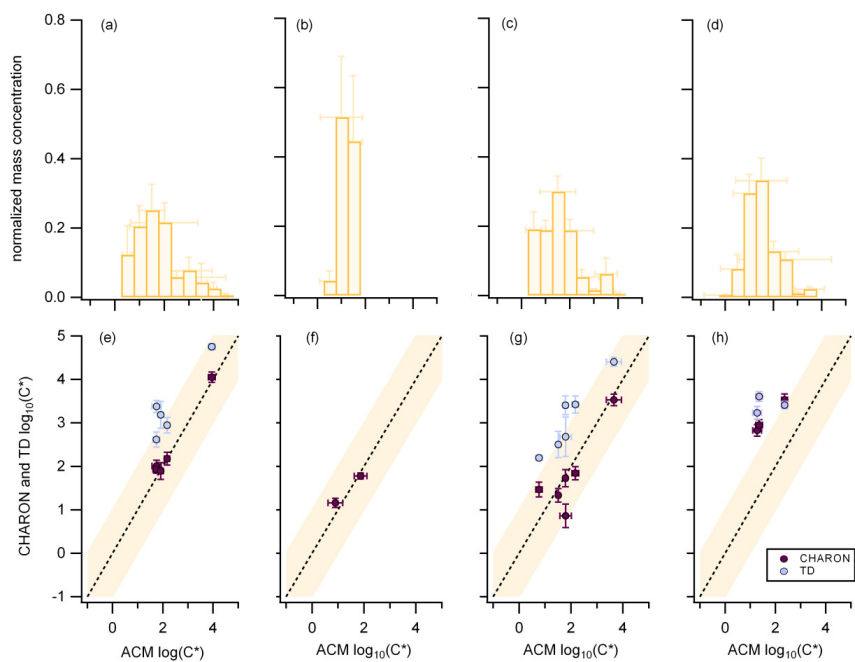
1108

1109

1110

1111

1112



1113

1114 **Figure 2:** Oxidation experiments using as precursor (1a,b,a,c) β -pinene, (2a,b,f) limonene, (3a,b,c,g) a mixture of β -pinene and
 1115 limonene and (4a,b,d,h) real tree emissions from *Pinus sylvestris* L. (Scots pine). Upper figures (1a, 2a, 3a, 4a, b, c, d) correspond
 1116 to the normalized average mass concentration from ACM, CHARON and TD, distributed to the different volatility bins with a
 1117 volatility resolution of $0.5 \mu\text{g m}^{-3}$. Bottom figures (1b, 2b, 3b, 4b, c, f, g, h) correspond to the average volatility of overlapping
 1118 compounds seen from CHARON and ACM (circles) or TD and ACM (double triangles). The dash line represents the 1:1 line. The
 1119 orange background color indicates the $\pm 1 \mu\text{g m}^{-3}$ deviation from the 1:1. Error bars correspond to the $\pm 1\sigma$ of the average
 1120 throughout each experiment.

1121

1122

1123

1124

1125

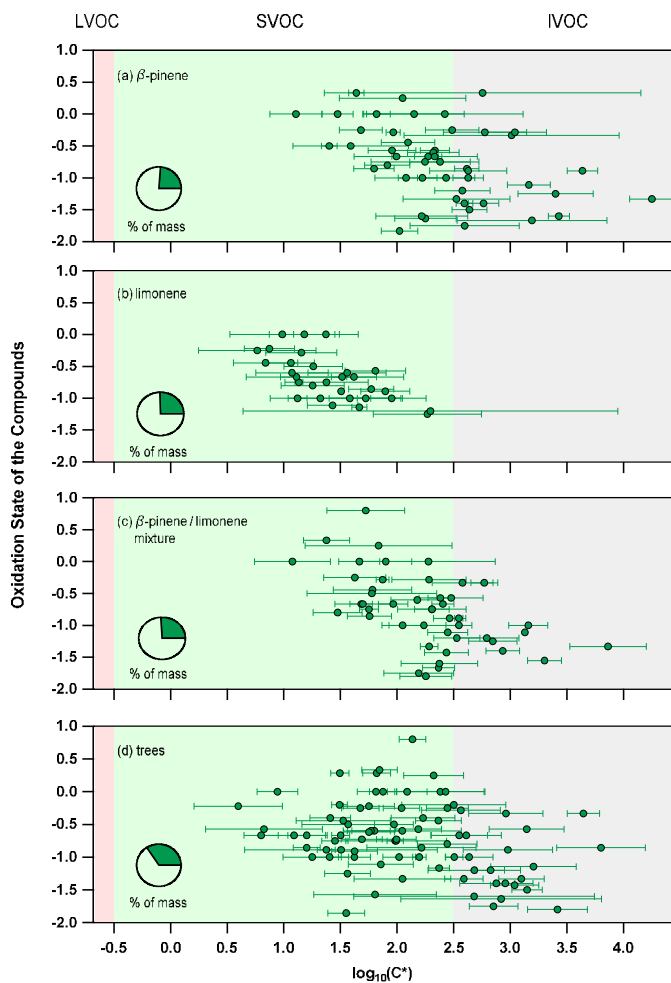
1126

1127

1128

1129

1130



1131

1132 Figure 3: The average experimental saturation concentration for detected ions (from ACM, CHARON or TD) that act as parent
 1133 ions identified using the described selection criteria during the (a) β -pinene, (b) limonene, (c) mixture of β -pinene and limonene
 1134 and (d) the real tree emissions experiments. Error bars indicate the $\pm 1\sigma$ of the experimental average. **Size of the markers are an**
 1135 **indicator of the oxygen atom number for each species.** Pie charts show the percent of mass (green) measured when adding all
 1136 presented ions compared to the total organic mass obtained from the AMS.

1137

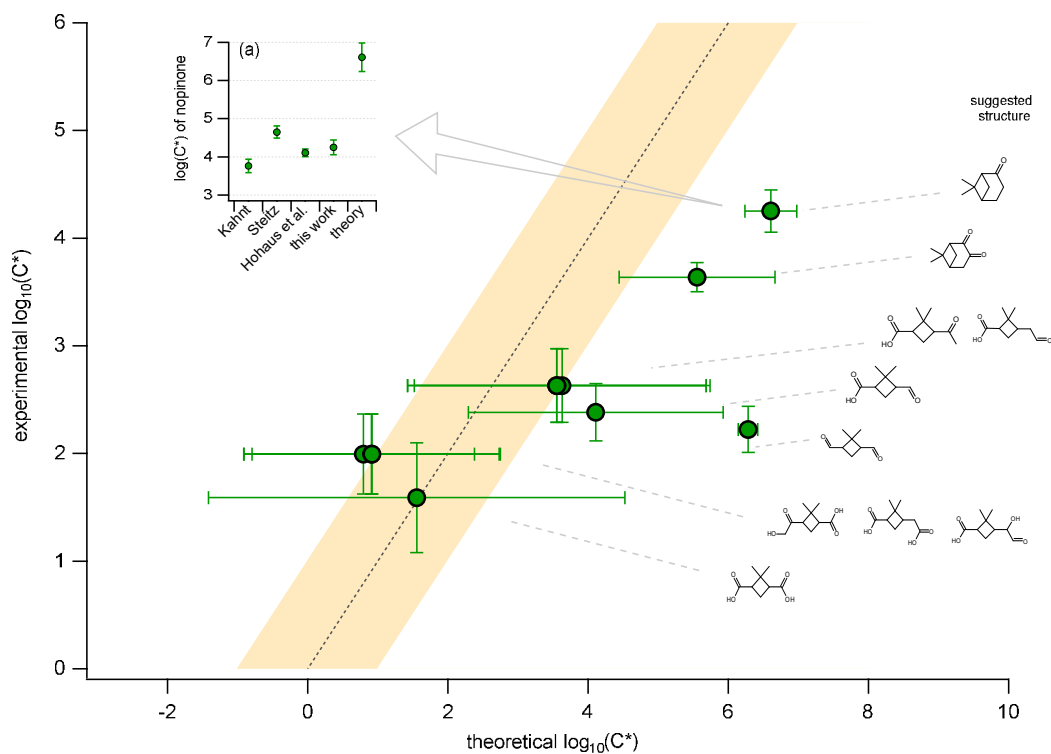
1138

1139

1140

1141

1142



1143

1144 **Figure 4:** The experimental average saturation concentration obtained from all PTR-based techniques (y-axis) compared to the
 1145 theoretical calculation of the saturation concentration (x-axis). Theoretical calculations were performed by assuming a chemical
 1146 structure for the experimentally observed ions. The chemical structure was attributed based on known oxidation products of the
 1147 β -pinene ozonolysis experiment and are shown on the right side of the figure. Error bars on the y-axis indicate the $\pm 1\sigma$ error of
 1148 the average based on the experimental results from ACM, TD and CHARON. The error bars for the x-axis act as indicators of the
 1149 minimum and maximum range of 9 different theoretical approaches with the position of the marker indicating the average of these
 1150 minimum and maximum values. More details on the theoretical calculations are provided in section 2.4. Sub-figure (a) provides
 1151 experimentally determined values of the saturation concentration for nopinone based on Hohaue et al. (2015) and Kahnt (2012)
 1152 together with the results of the experimental and theoretical approaches from this study.

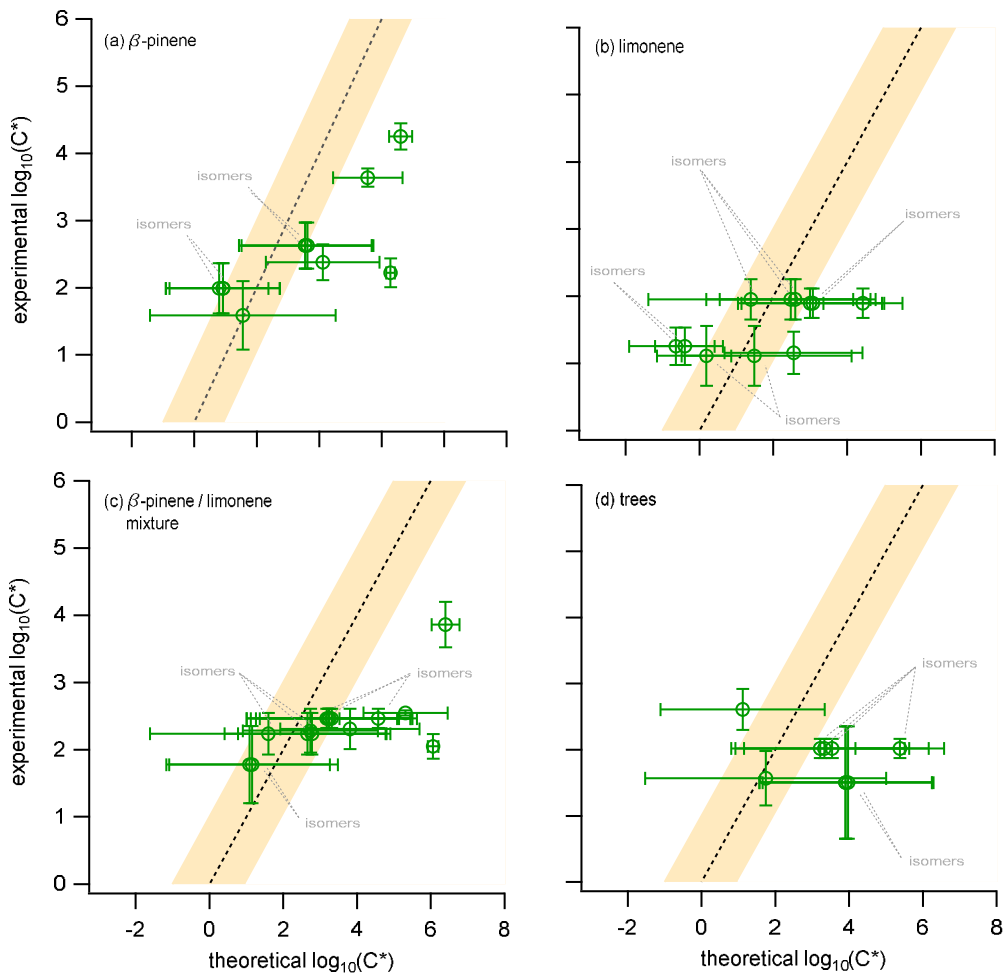
1153

1154

1155

1156

1157



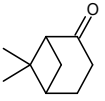
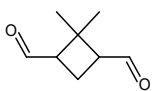
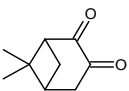
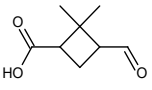
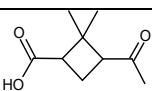
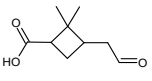
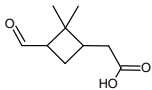
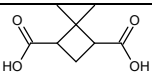
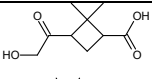
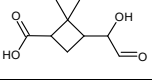
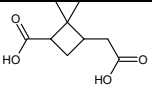
1158

1159 **Figure 5: The experimental average saturation concentration obtained from all PTR-based techniques (y-axis) compared to the**
 1160 **theoretical calculation of the saturation concentration (x-axis) for the (i) β -pinene, (ii) limonene, (iii) mixture of β -pinene and**
 1161 **limonene and (iv) the real tree emissions experiments. Error bars on the y-axis indicate the $\pm 1\sigma$ error of the average based on the**
 1162 **experimental results from ACM, TD and CHARON. The error bars for the x-axis act as indicators of the minimum and maximum**
 1163 **range of 9 different theoretical approaches with the position of the marker indicating the average of these minimum and maximum**
 1164 **values.**

Supplementary material for the publication:

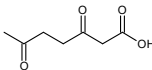
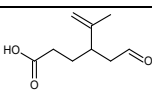
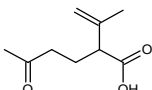
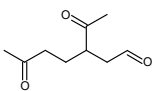
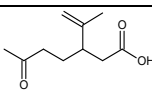
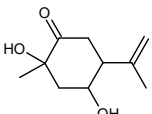
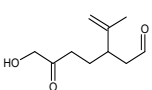
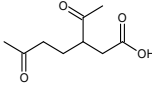
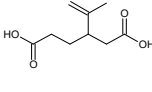
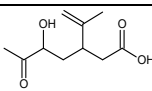
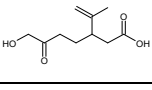
Gas-to-particle partitioning of major biogenic oxidation products from monoterpenes and real plant emissions

Table S1: Major compounds identified as parent ions from the PTR-based techniques that have been observed in previous publications. Suggested names and structures are attributed to the chemical formula that was identified by the PTR-based techniques.

	Chemical formula	MW	Structure	SMILES code
β-pinene				
(Hohaus et al., 2015; Chen and Griffin, 2005; Jenkin, 2004; Yu et al., 1999)				
Nopinone	C ₉ H ₁₄ O	138.21		CC1(C2CC1C(=O)CC2)C
2,2-Dimethyl-cyclobutane-1,3-dicarboxaldehyde	C ₈ H ₁₂ O ₂	140.18		O=CC1CC(C=O)C1(C)C
Oxonopinone	C ₉ H ₁₂ O ₂	152.19		CC1(C2CC1C(=O)C(=O)C2)C
2,2-Dimethyl-3-formyl-cyclobutyl-methanoic acid	C ₈ H ₁₂ O ₃	156.18		OC(=O)C1CC(C=O)C1(C)C
				OC(=O)C1CC(C(C)=O)C1(C)C
Norpinonic acid top/ Pinalic-3-acid middle/ Pinalic-4-acid bottom	C ₉ H ₁₄ O ₃	170.21	 	OC(=O)C1CC(CC=O)C1(C)C OC(=O)CC1CC(C=O)C1(C)C
Norpinic acid	C ₈ H ₁₂ O ₄	172.18		CC1(C(CC1C(=O)O)C(=O)O)C
Hydroxy norpinonic acids	C ₉ H ₁₄ O ₄	186.21	 	OC(=O)C1CC(C(=O)CO)C1(C)C OC(C=O)C1CC(C(=O)O)C1(C)C
Pinic acid	C ₉ H ₁₄ O ₄	186.21		CC1(C(CC1C(=O)O)CC(=O)O)C

Limonene

(Kundu et al., 2012;Jaoui et al., 2006;Chen and Griffin, 2005;Leungsakul et al., 2005b;Leungsakul et al., 2005a)

3,6-Oxoheptanoic acid	C ₇ H ₁₀ O ₄	158.15		O=C(CCC(C)=O)CC(=O)O
				O=CCC(CCC(=O)O)C(=C)C
Limonic acid/ Norlimononic acid/ Ketolimononaldehyde	C ₉ H ₁₄ O ₃	170.21		O=C(C)CCC(C(=C)C)C(=O)O
				CC(=O)C(CC=O)CCC(=O)C
				O=C(C)CCC(CC(=O)O)C(=C)C
Limonic acid/ 4-Isopropenyl-1-methyl-1,5- hydroxy-2-oxocyclohexane/ 7-Hydroxylimononaldehyde	C ₁₀ H ₁₆ O ₃	184.23		CC(=C)C1CC(=O)C(C)(O)CC1O
				O=C(CCC(CC=O)C(=C)C)CO
Ketolimononic acid/ Limonic acid	C ₉ H ₁₄ O ₄	186.21		O=C(C)CCC(CC(=O)O)C(C)=O
				OC(=O)CCC(CC(=O)O)C(=C)C
5-Hydroxylimononic acid/ 7-Hydroxylimononic acid	C ₁₀ H ₁₆ O ₄	200.23		O=C(C)C(O)CC(CC(O)=O)C(=C)C
				O=C(CCC(CC(=O)O)C(=C)C)CO

Trees

(α -pinene / Δ^3 -carene)

(Praplan et al., 2014;Chen and Griffin, 2005;Yu et al., 1999)

3-Norcaronic acid and isomers	C ₉ H ₁₄ O ₃	170.21	O=C(C)CC1C(C(=O)O)C1(C)C
-------------------------------	---	--------	--------------------------

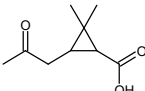
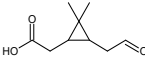

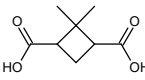
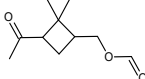
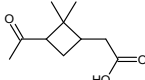
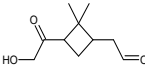
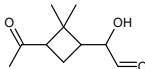
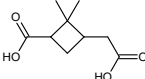
				<chem>OC(=O)CC1C(CC=O)C1(C)C</chem>
				<chem>OC(=O)CC1C(CC=O)C1(C)C</chem>
				
Norpinic acid / Nor-3-caric acid	$C_8H_{12}O_4$	172.18		<chem>CC1(C(CC1C(=O)O)C(=O)O)C</chem>
				<chem>O=C(C)C1CC(COC=O)C1(C)C</chem>
2,2-Dimethyl-3-formyl-cyclobutyl-methanoic-acid/ Pinonic acid / 3-caronic acid/ Hydroxy pinonaldehydes	$C_{10}H_{16}O_3$	184.23		<chem>OC(=O)CC1CC(C(C)=O)C1(C)C</chem>
				<chem>O=C(CO)C1CC(CC=O)C1(C)C</chem>
				<chem>OC(C=O)C1CC(C(C)=O)C1(C)C</chem>
Pinic acid / 3-Caric acid	$C_9H_{14}O_4$	186.21		<chem>CC1(C(CC1C(=O)O)CC(=O)O)C</chem>

Table S1: Instruments operating conditions as described in Gkatzelis et al. (2018).

<u>INSTRUMENT CHARACTERISTICS</u>	<u>ACM (in situ)</u>	<u>CHARON (online)</u>	<u>TD (in situ)</u>
<u>Time resolution (min)</u>	<u>240</u>	<u>1</u>	<u>120</u>
<u>Gas/particle separation</u>	<u>High vacuum</u>	<u>Denuder</u>	<u>Denuder and/or blank correction (filtered air)</u>
<u>Pre-concentration factor</u>	<u>21^a</u>	<u>44</u>	<u>6000^b</u>
<u>LOD^c (ng/m³)</u>	<u>35^d</u>	<u>1.4^c</u>	<u>0.02^b</u>
<u>Temperature range (°C)</u>	<u>25 – 250</u>	<u>140</u>	<u>25 – 350</u>
<u>Heating rate (°C / min)</u>	<u>100</u>	<u>0</u>	<u>15</u>
<u>Temperature steps (°C)</u>	<u>100, 150, 250 (3 min)</u>	<u>none</u>	<u>None</u>
<u>Desorption pressure (atm)</u>	<u>1</u>	<u><1</u>	<u>1</u>
<u>Particle range (nm)</u>	<u>70 – 1000</u>	<u>70 – 1000</u>	<u>70 - 2000</u>
<u>PTR-ToF-MS model</u>	<u>8000</u>	<u>8000</u>	<u>8000</u>
<u>Drift tube Temperature (°C) / Pressure (mbar) / Voltage (V)</u>	<u>90 / 2.3 / 550</u>	<u>120 / 2.4 / 400 and 240</u>	<u>120 / 2.25 / 600</u>
<u>PTR-ToF-MS E/N (Td)</u>	<u>120</u>	<u>65 / 100</u>	<u>160</u>
<u>PTR-ToF-MS mass resolution (m/Δm)</u>	<u>2500</u>	<u>4500-5000</u>	<u>4000</u>

^a based on 240 min sampling at 80 mL/min and 3 min desorption at 300 mL/min

^b based on 30 min sampling at 6 L/min and 3 min desorption at 10 mL/min a typical value for most ions based on the method in (Holzinger et al., 2010)

^c Limit of detection

^d For signal on m/z 139 and 10 sec integration time

^e For signals around m/z 200 and 1 min integration time

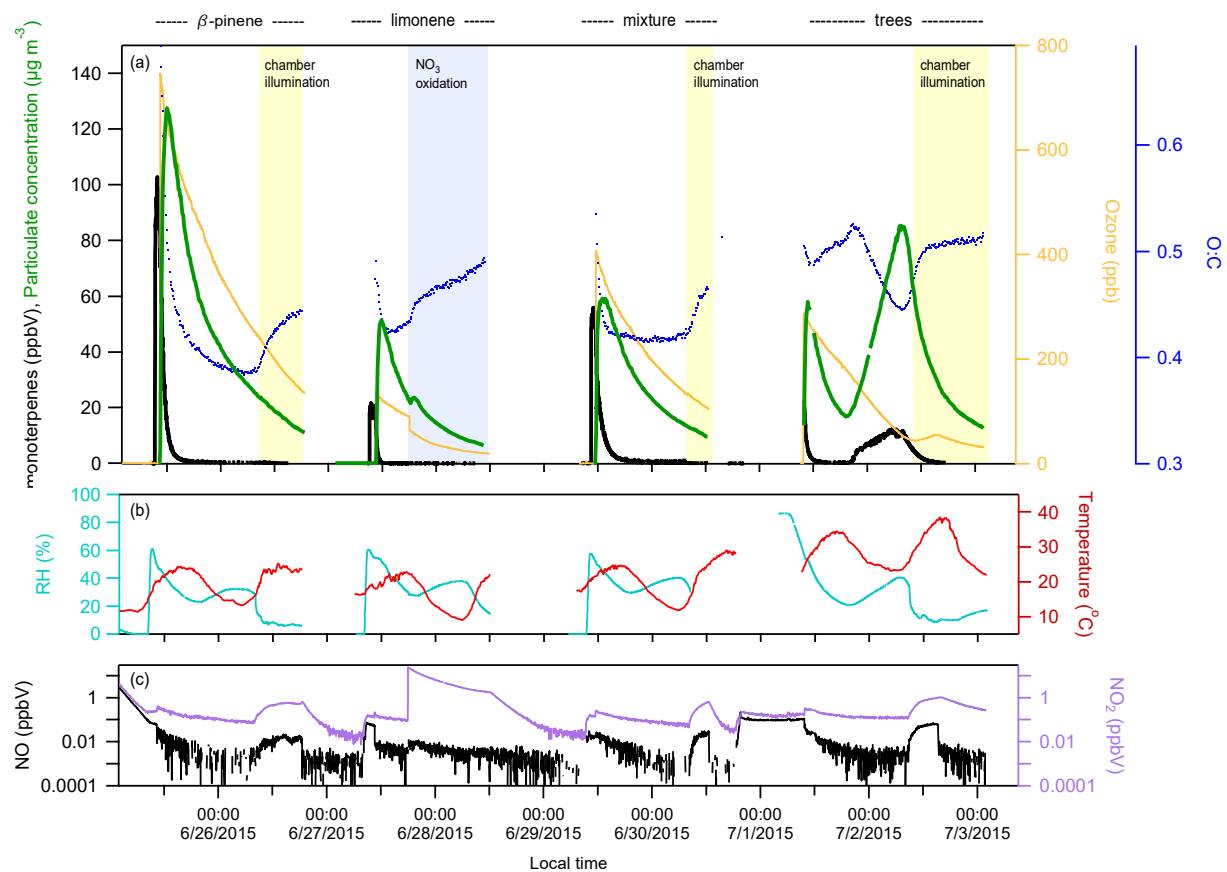


Figure S1: An overview of all experiments during the campaign with (a) corresponding to the mixing ratios of the injected monoterpenes (black line) and ozone (orange line) as well as the SOA mass produced (green line) and its O:C ratio as an indicator of the oxidation of the SOA. Background colours correspond to the opening of the roof (yellow) or the NO₃ oxidation initiation (blue colour). Measurement of the RH (ciel), temperature (red), NO (black) and NO₂ (purple) are also provided.

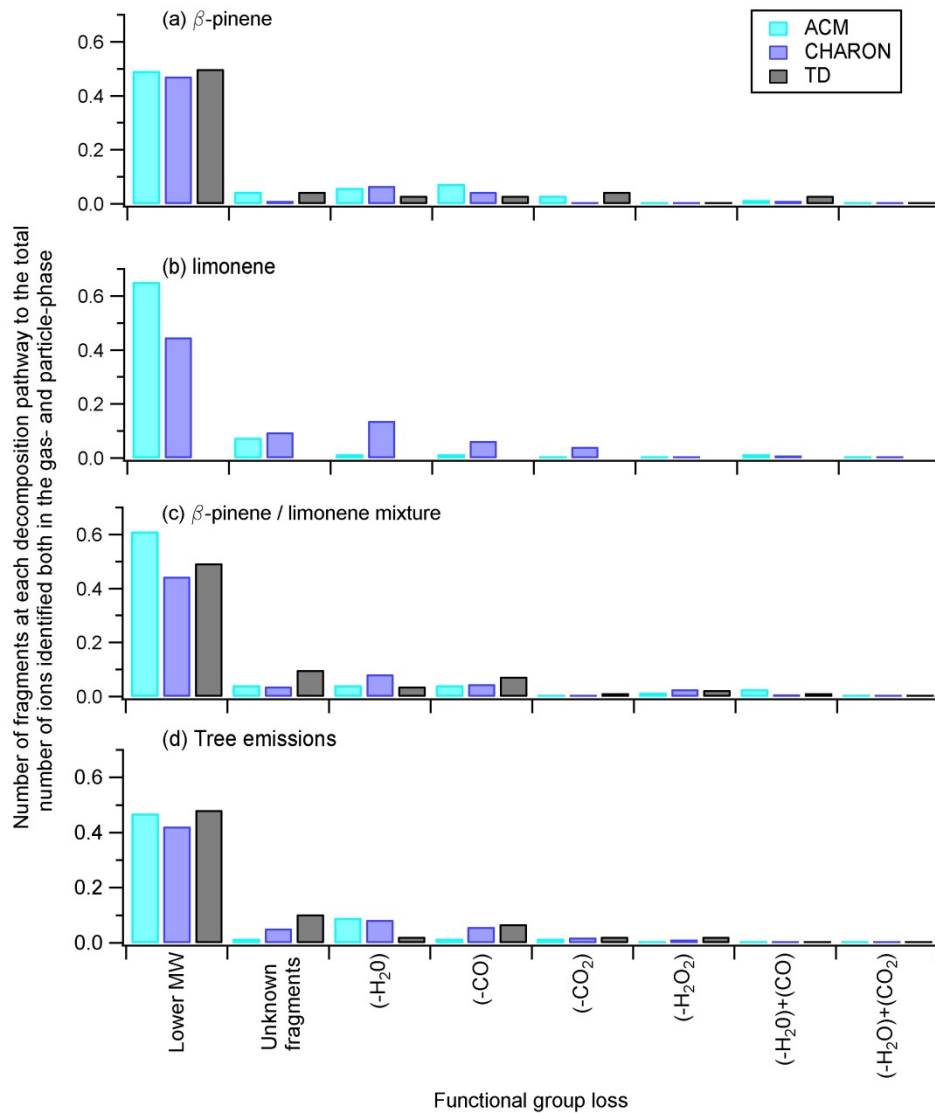


Figure S2: The ratio of the number of lower molecular weight and unknown fragments as well as fragments subject to functional group loss ((-H₂O), (-CO) (-CO₂), (-H₂O₂), (-H₂O) and (-CO), (-H₂O) and (-CO₂)) to the number of identified ions both in the gas- and particle-phase. Different colours indicate the different instruments for the different experiments.

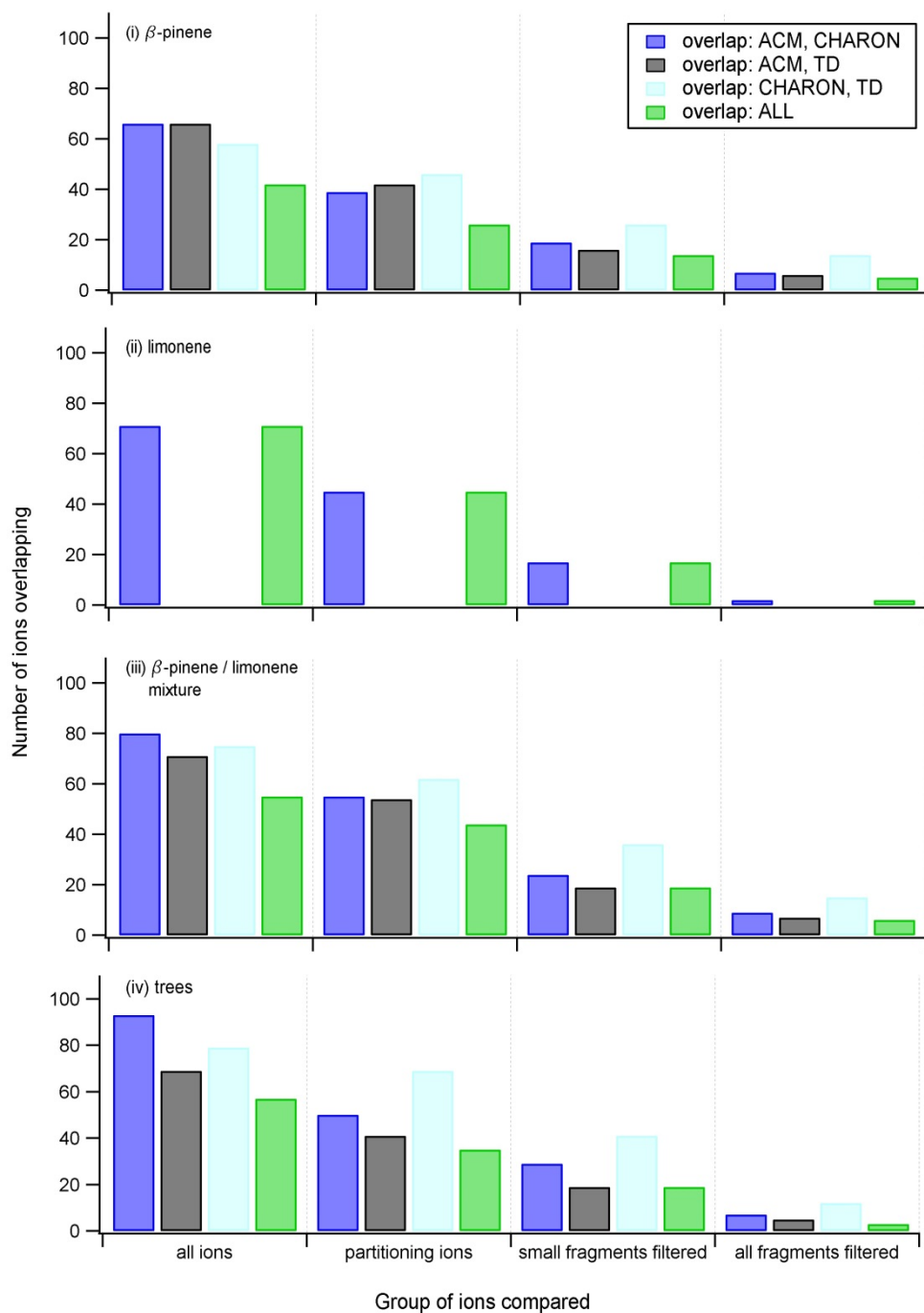


Figure S3: The number of ions measured from more than one technique with a focus on the ions measured both from ACM and CHARON (blue), ACM and TD (black), CHARON and TD (ciel) and ions measured from all techniques, accounting for ACM, TD and CHARON (green). Overlaps are checked for different groups of ions starting from the overlaps of all ions detected, to overlaps seen for only the ions that partition between the gas- and particle-phase, to the overlaps of the remaining partitioning ions after filtering out the small fragments and the remaining partitioning ions after filtering out all fragments for the different experiments performed.

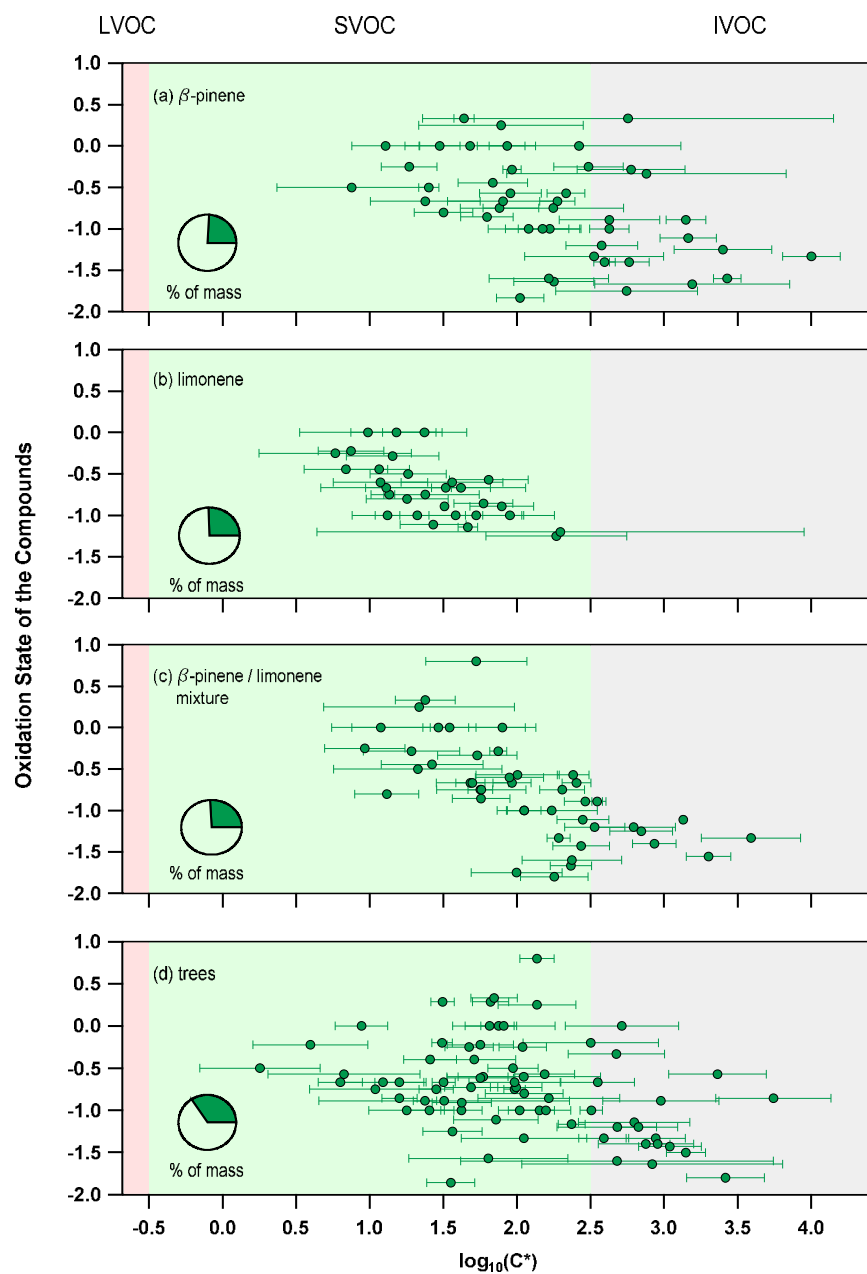


Figure S4: The average experimental saturation concentration for detected ions (from ACM and CHARON) that act as parent ions identified using the described selection criteria during the different experiments. Error bars indicate the $\pm 1\sigma$ of the average. Size of the markers is an indicator of the oxygen atom number for each species. Pie charts show the percent of mass (green) measured when adding all presented ions compared to the total organic mass obtained from the AMS.

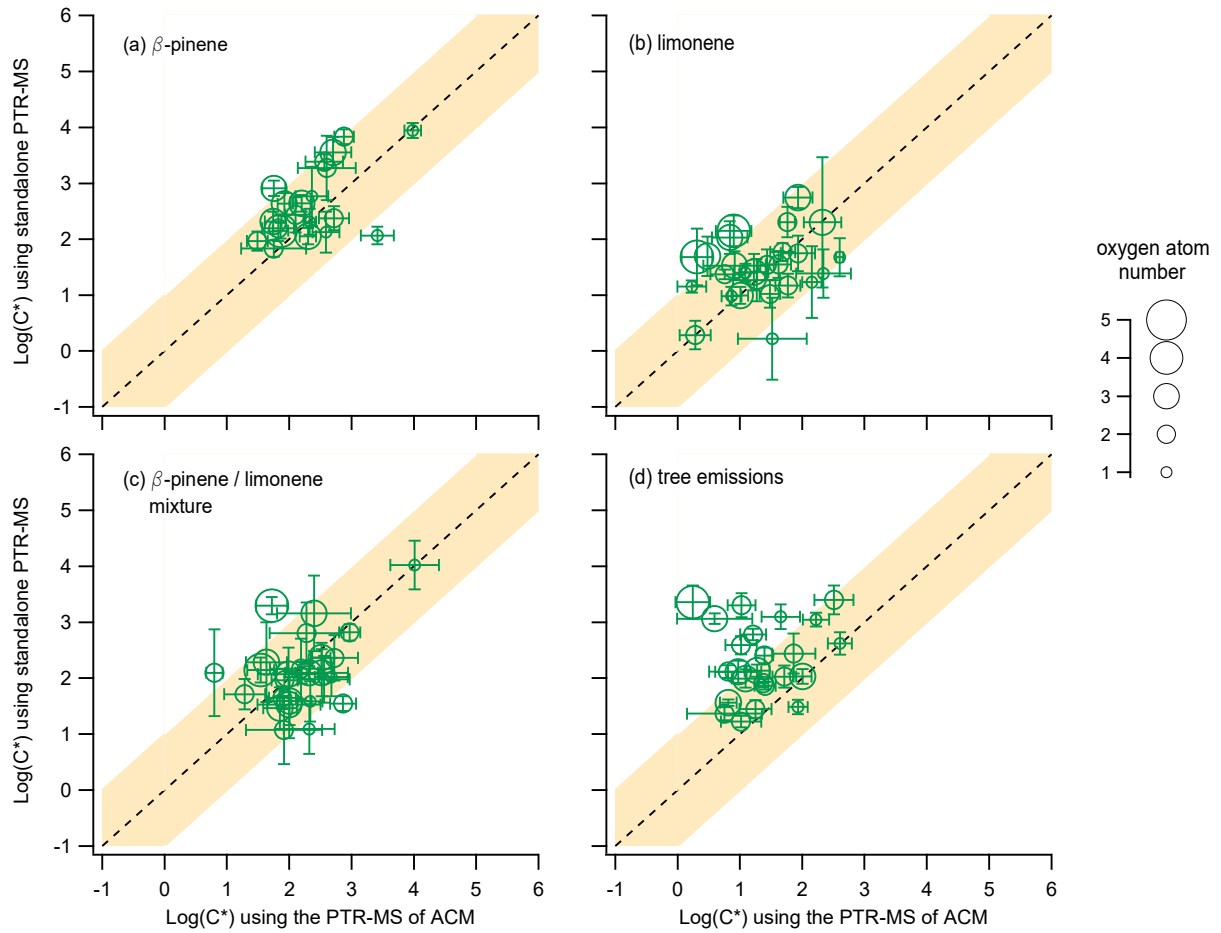


Figure S5: The average saturation mass concentration from the individual experiments for the ACM when using the gas-phase mass concentration values obtained from the PTR-MS of ACM (x-axis) in comparison to the standalone PTR-MS (y-axis). Error bars indicate the $\pm 1\sigma$ of the average. Size of the markers is an indicator of the oxygen atom number for each species.

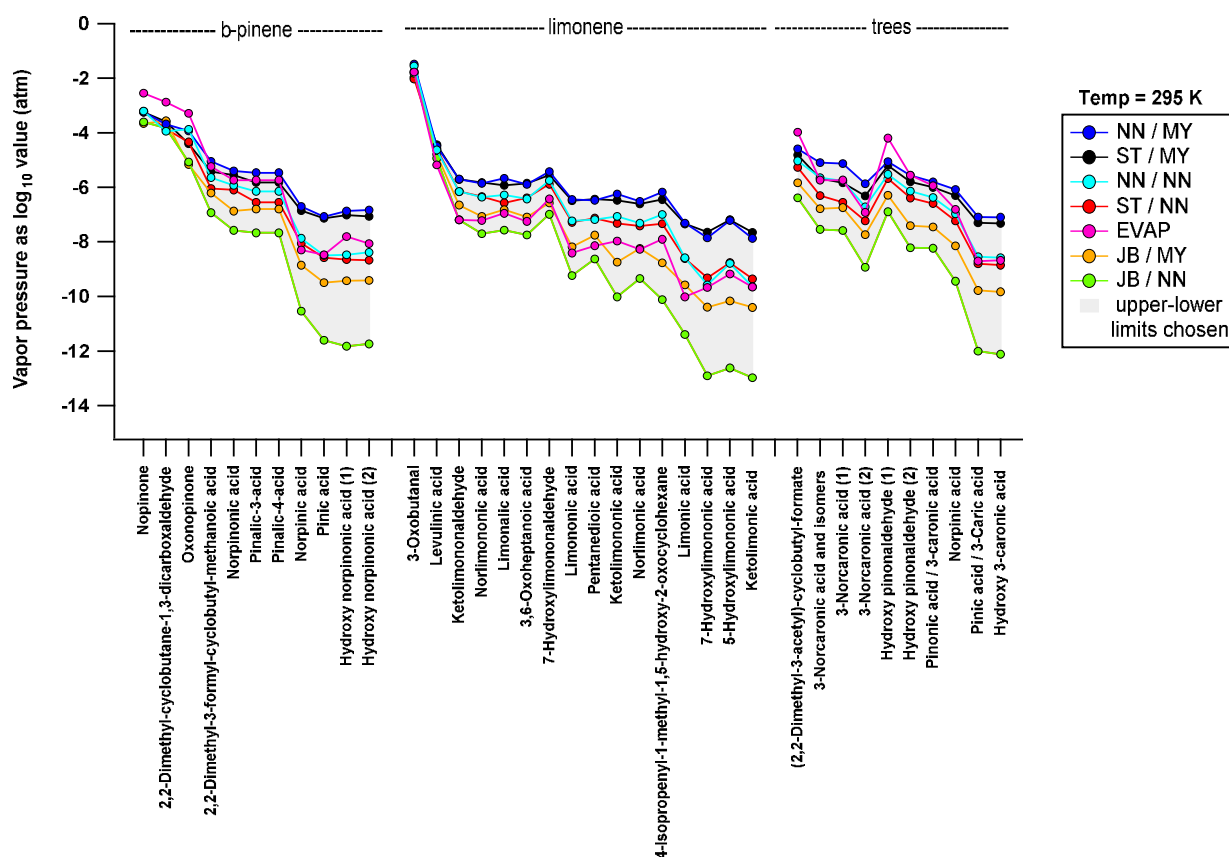


Figure S6: Theoretical calculation of the vapor pressure (y-axis) using the combination of 7 different approaches. The grey background color indicates the minimum and maximum range chosen for this study. Details on the different approaches are provided in section 2.4 [and below](#).

[The method originally proposed by Joback and Reid \(1987\) to predict boiling points based on the molecular structure of the investigated compounds explicitly treats ring increments, which are relevant to monoterpene calculations and thus for this study. Nannoolal et al. \(2004\) extended the investigated range of functional groups, simultaneously introducing information on a greater neighborhood of the central atom of the investigated functional group. The \$T_B\$ function fitted to the chosen experimental dataset -enlarged as well - yielded lower boiling points for the compounds investigated here, associated with higher vapor pressure. The method developed by Myrdal and Yalkowsky \(1997\) includes heat capacity changes for phase transitions into their empirical representation, yielding a lowering in the vapor pressure estimates, compared with the approaches used hitherto \(Camredon et al., 2010\). The dependency of \$\Delta C_p\$ upon molecular flexibility, i.e. the number of torsional bonds \(nonterminal \$sp^3\$ and \$sp^2\$, rings\), makes this inclusion very interesting for monoterpene calculations. Nannoolal et al. \(2008\) accounted for the heat capacity changes upon vaporization, too. The new feature here is that non-additive interaction contribution of multi-functional groups \(e.g. OH-ketone\) are adopted, resulting in lower vapor pressure values compared with the previous methods. Higher electron delocalization induce stronger dispersive forces, thus decreasing the \$p_{i,L}\$. This might explain the larger discrepancy between the vapor pressure values calculated by NN/MY and JB/NN with the increasing of alcohol/carbonyl/carboxyl functional group number.](#)

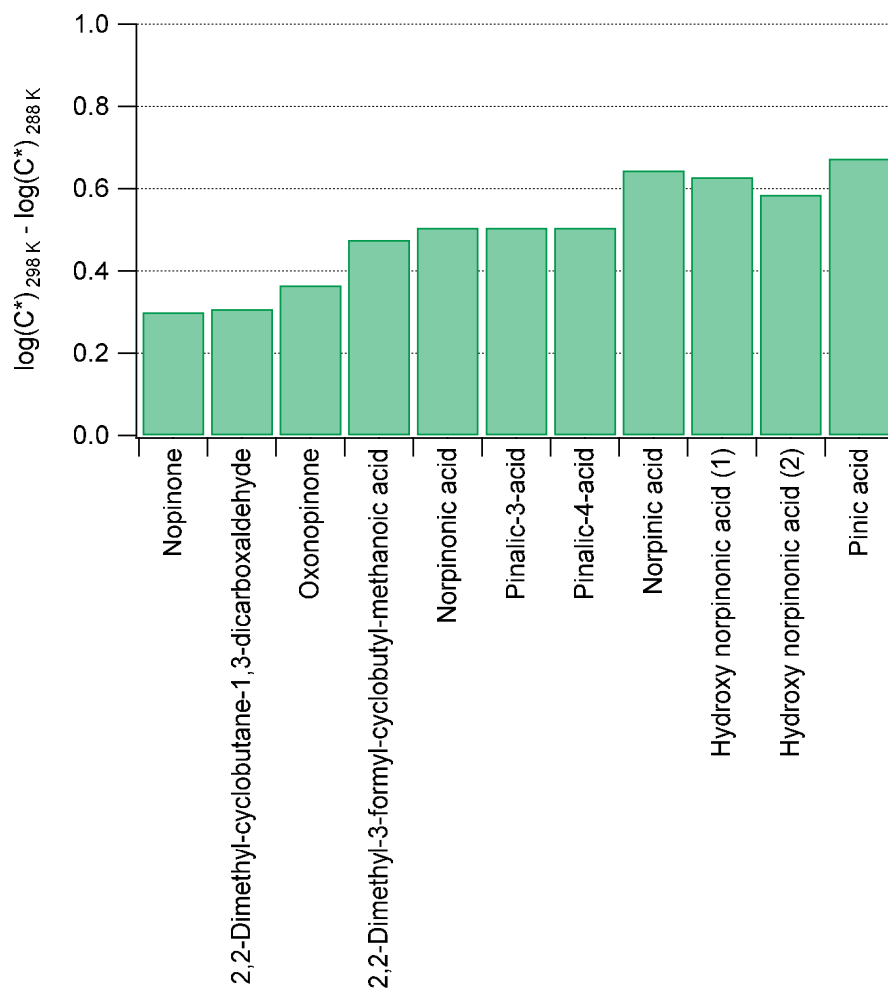


Figure S7: Theoretical calculation of the vapor pressure (y-axis) using the combination of 7 different approaches. To estimate the uncertainty in the experiments due to changes in temperature calculations were also performed at 295 K. Difference in vapor pressure are between 0.3 to 0.6 $\log(C^*)$.

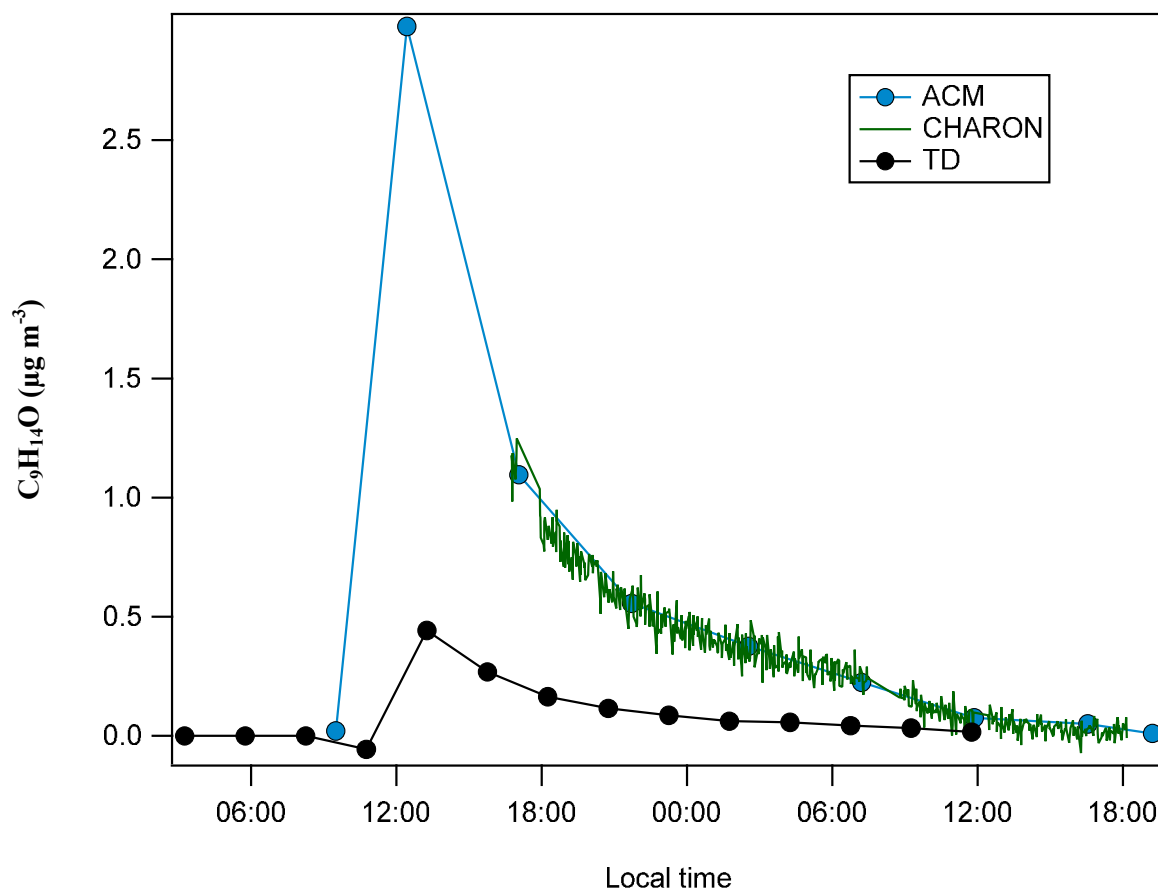


Figure S8: Characteristic example of the timeseries of $C_9H_{14}O$ for the three different inlet techniques

References

- Camredon, M., Hamilton, J. F., Alam, M. S., Wyche, K. P., Carr, T., White, I. R., Monks, P. S., Rickard, A. R., and Bloss, W. J.: Distribution of gaseous and particulate organic composition during dark alpha-pinene ozonolysis, *Atmos Chem Phys*, 10, 2893-2917, DOI 10.5194/acp-10-2893-2010, 2010.
- Chen, J., and Griffin, R.: Modeling secondary organic aerosol formation from oxidation of α -pinene, β -pinene, and limonene, *Atmos Environ*, 39, 7731-7744, 10.1016/j.atmosenv.2005.05.049, 2005.
- Gkatzelis, G. I., Tillmann, R., Hohaus, T., Müller, M., Eichler, P., Xu, K. M., Schlag, P., Schmitt, S. H., Wegener, R., Kaminski, M., Holzinger, R., Wisthaler, A., and Kiendler-Scharr, A.: Comparison of three aerosol chemical characterization techniques utilizing ptr-tof-ms: A study on freshly formed and aged biogenic soa, *Atmos. Meas. Tech.*, 11, 1481-1500, 10.5194/amt-11-1481-2018, 2018.
- Hohaus, T., Gensch, I., Kimmel, J. R., Worsnop, D. R., and Kiendler-Scharr, A.: Experimental determination of the partitioning coefficient of β -pinene oxidation products in soas, *Phys Chem Chem Phys*, 17, 14796-14804, 10.1039/C5CP01608H, 2015.
- Holzinger, R., Kasper-Giebl, A., Staudinger, M., Schauer, G., and Rockmann, T.: Analysis of the chemical composition of organic aerosol at the mt. Sonnblick observatory using a novel high mass resolution thermal-desorption proton-transfer-reaction mass-spectrometer (hr-td-ptr-ms), *Atmos Chem Phys*, 10, 10111-10128, DOI 10.5194/acp-10-10111-2010, 2010.
- Jaoui, M., Corse, E., Kleindienst, T. E., Offenberg, J. H., Lewandowski, M., and Edney, E. O.: Analysis of secondary organic aerosol compounds from the photooxidation of d-limonene in the presence of nox and their detection in ambient pm2.5, *Environ Sci Technol*, 40, 3819-3828, 10.1021/es052566z, 2006.
- Jenkin, M. E.: Modelling the formation and composition of secondary organic aerosol from α - and β -pinene ozonolysis using mcm v3 *Atmos Chem Phys*, 4, 1741-1757, 2004.
- Joback, K. G., and Reid, R. C.: Estimation of pure-component properties from group-contributions, *Chemical Engineering Communications*, 57, 233-243, 10.1080/00986448708960487, 1987.
- Kundu, S., Fisseha, R., Putman, A. L., Rahn, T. A., and Mazzoleni, L. R.: High molecular weight soa formation during limonene ozonolysis: Insights from ultrahigh-resolution ft-icr mass spectrometry characterization, *Atmos Chem Phys*, 12, 5523-5536, 10.5194/acp-12-5523-2012, 2012.
- Leungsakul, S., Jaoui, M., and Kamens, R. M.: Kinetic mechanism for predicting secondary organic aerosol formation from the reaction of d-limonene with ozone, *Environ Sci Technol*, 39, 9583-9594, 10.1021/es0492687, 2005a.
- Leungsakul, S., Jeffries, H. E., and Kamens, R. M.: A kinetic mechanism for predicting secondary aerosol formation from the reactions of d-limonene in the presence of oxides of nitrogen and natural sunlight, *Atmos Environ*, 39, 7063-7082, 10.1016/j.atmosenv.2005.08.024, 2005b.
- Myrdal, P. B., and Yalkowsky, S. H.: Estimating pure component vapor pressures of complex organic molecules, *Ind Eng Chem Res*, 36, 2494-2499, 10.1021/ie950242l, 1997.
- Nannoolal, Y., Rarey, J., Ramjugernath, D., and Cordes, W.: Estimation of pure component properties: Part 1. Estimation of the normal boiling point of non-electrolyte organic compounds via group contributions and group interactions, *Fluid Phase Equilibria*, 226, 45-63, <https://doi.org/10.1016/j.fluid.2004.09.001>, 2004.
- Nannoolal, Y., Rarey, J., and Ramjugernath, D.: Estimation of pure component properties: Part 3. Estimation of the vapor pressure of non-electrolyte organic compounds via group contributions and group interactions, *Fluid Phase Equilibria*, 269, 117-133, <https://doi.org/10.1016/j.fluid.2008.04.020>, 2008.
- Praplan, A. P., Schobesberger, S., Bianchi, F., Rissanen, M. P., Ehn, M., Jokinen, T., Junninen, H., Adamov, A., Amorim, A., Dommen, J., Duplissy, J., Hakala, J., Hansel, A., Heinritzi, M., Kangasluoma, J., Kirkby, J., Krapf, M., Kürten, A., Lehtipalo, K., Riccobono, F., Rondo, L., Sarnela, N., Simon, M., Tomé, A., Tröstl, J., Winkler, P. M., Williamson, C., Ye, P., Curtius, J., Baltensperger, U., Donahue, N. M., Kulmala, M., and Worsnop, D.

R.: Elemental composition and clustering of α -pinene oxidation products for different oxidation conditions, Atmos Chem Phys Disc, 14, 30799-30833, 10.5194/acpd-14-30799-2014, 2014.

Yu, J., Cocker, D. R., Griffin, R. J., Flagan, R. C., and Seinfeld, J. H.: Gas-phase ozone oxidation of monoterpenes: Gaseous and particulate products, J Atmos Chem, 34, 207-258, 10.1023/a:1006254930583, 1999.